Title
Development of Advanced Secondary Zinc Cells for Power-Source Applications

Authors
Chen, J.-S.
McLarnon, F.R.
Cairns, E.J.

Publication Date
1991-12-01

LBL-31931
UC-210

Lawrence Berkeley Laboratory
UNIVERSITY OF CALIFORNIA

ENERGY & ENVIRONMENT DIVISION

Development of Advanced Secondary Zinc Cells for Power-Source Applications

J.-S. Chen, F.R. McLarnon, and E.J. Cairns

December 1991

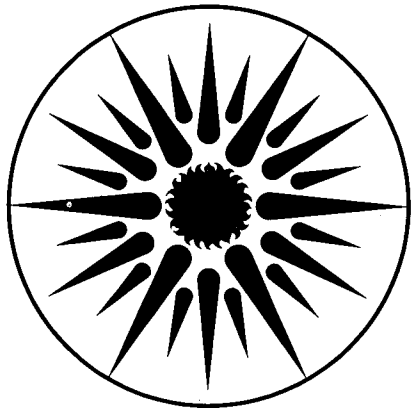

ENERGY & ENVIRONMENT DIVISION

Prepared for the U.S. Department of Energy under Contract Number DE-AC03-76SF00098

DISCLAIMER

LBL-31931

DEVELOPMENT OF ADVANCED SECONDARY ZINC CELLS FOR POWER-SOURCE APPLICATIONS

Jenn-Shing Chen, Frank R. McLarnon and Elton J. Cairns

Energy & Environment Division
Lawrence Berkeley Laboratory
Berkeley, CA 94720

December 1991

Sponsored by:

Defense Advanced Research Projects Agency (DoD)
Undersea Warfare Office
Submarine Technology Program
Mechanical and Electrical Area

for

Naval Sea Systems Command

This work was supported by the Defense Advanced Research Projects Agency, Undersea Warfare Office, Submarine Technology Program, under ARPA Order Number MIPR N0002490MP70004, through the U.S. Department of Energy under Contract No. DE-AC01-76SF00098.

INTRODUCTION

The general advantages of Zn/AgO batteries are high specific energy, high discharge rate capability, good charge acceptance, and low self-discharge rate. However, the principal disadvantages of high cost and short cycle life have limited the use of this battery to applications where high specific energy is the prime requisite, such as military and flight applications, portable electronic equipment, *etc.* The major objectives of this research project are to improve the Zn/AgO cell cycle life and increase its performance. The redistribution of Zn active material (shape change) and the growth of Zn dendrites (which leads to cell shorting) have been identified as primary factors that limit the cycle-life performance of Zn/AgO cells. These phenomena can be largely overcome by improvements in separator materials, and by additives to the electrode and electrolyte. Recent development work on Zn/AgO cells has been concentrated in the area of Zn electrode and separator improvements to extend the lifetimes of cells [1,2]. It is well known that shape change and dendrite problems can be attributed to the high solubility of the ZnO discharge product in concentrated KOH electrolyte. Because the ZnO solubility depends strongly on the KOH concentration, a useful strategy is to operate the cell at as low a KOH concentration as can be tolerated by the positive electrode, and add indifferent supporting electrolyte to maintain acceptable ionic conductivity. Much research has successfully applied different alternative electrolytes, such as those containing fluoride, borate, phosphate, arsenate, and carbonate ions, to extend Zn/NiOOH cell cycle life [3]. In this work, the primary objective was to determine the ability of reduced-zinc-solubility electrolytes to extend the cycle life of Zn/AgO cells by additives (F^-, CO_3^{2-}, BO_3^{3-}, PO_4^{3-}) to the KOH electrolyte.

Many investigations have shown that the addition of $Ca(OH)_2$ to the zinc electrode can reduce the zincate-ion [$Zn(OH)_4^{2-}$] solubility and thereby improve the cycle life of Zn/NiOOH cells [3 - 5]. When $Ca(OH)_2$ is added to ZnO in alkaline electrolyte, an insoluble calcium zin-

cate compound, $Ca(OH)_2 \cdot 2Zn(OH)_2 \cdot 2H_2O$, is formed, thereby "trapping" the soluble $K_2Zn(OH)_4$ species [6]. Therefore, in this research the other objective is to determine the ability of calcium-containing zinc electrodes to extend the cycle life of Zn/AgO cells.

EXPERIMENTAL PROCEDURES

In this work, two group of cells were tested. One group of cells was fabricated by BST, Inc. and the other group was fabricated by LBL.

(1) Cell construction: All cells were designed to be silver-limiting in capacity, and deliver 5-Ah of rated capacity. The electrode sizes were 1.75" x 1.4". In order to use the BST-fabricated AgO electrodes and cell cases, each cell contained six AgO electrodes, five full-capacity Zn electrodes, and two half-capacity Zn electrodes which were used as the outermost electrodes in the cell pack. The detailed cell-design calculations are presented in the Appendix. Table I summarizes the cell design for the BST and LBL cell groups. The BST cell group consisted of six BST-fabricated Zn/AgO cells and the LBL cell group included five LBL-fabricated Zn/AgO cells and two LBL-fabricated ZnCa/AgO cells.

(2) Electrode specifications: All positive electrodes used in this work were furnished by BST, Inc. Each positive electrode contained 2.58 g Ag applied on a Ag mesh current collector and was ~0.015" thick. In the BST-cell group, each full-capacity negative electrode contained 3.66 g ZnO applied to a Ag sheet current collector and was about 0.035" thick. In the LBL-cell group, the negative electrodes were prepared by a vacuum-table process [7]. Figure 1 shows the flow chart of this process for fabricating Zn electrodes. Each electrode contained 3.7 g ZnO and was ~0.048" thick. The electrode compositions were: 93 wt% ZnO (Mallinckrodt, Inc., Paris, KY, 99.9% pure), 2 wt% PbO (Mallinckrodt, Inc., 99% pure), 4 wt% PTFE (E.I. Dupont de Nemours and Co., Wilmington, DE, Teflon Type 30 dispersion), and 1 wt% Coronado newsprint (The Morilla Company, Los Angeles, CA). An 0.55-mm dia. Ag wire (Johnson Matthey/

TABLE I : Zn/AgO Cell Design (silver-limiting capacity design)

	BST	LBL
Rated Capacity	5 Ah	5 Ah
Electrode size (each plate)	1.75" x 1.4 "	1.75" x 1.4"
Weight of Zn or Ag / Cell	ZnO = 21.96 g Ag = 15.48 g	Zn- ZnO = 22.2 g ZnCa - ZnO = 17.03 g $Ca(OH)_2$ = 5.17 g Ag = 15.48 g
Ratio of active materials	Mzn/Mag Mass Ratio = 1.14	Zn - Mzn/Mag Ratio = 1.15 ZnCa - Mzn/Mag Ratio = 0.88
Porosity (as metal based)	ZnO = 50-60 % Ag = 55-60 %	ZnO = 65-70 %, ZnCa = 65-70 % Ag = 55-60 %
Cell pack	7 - ZnO, 6 - Ag, 12 - Sep.	7 - ZnO, 6 - Ag, 12 - Sep.
Separator system	-/dexter//5*cp/cg/pellon/+	-/2*cg//5*cp/cg/pellon/+
Thickness for each plate	ZnO = 0.089 cm (35 mils) Ag = 0.038 cm (15 mils)	ZnO = 0.122 cm (48 mils) ZnCa = 0.175 cm (67 mils) Ag = 0.038 cm (15 mils)
Total Thickness of Cell	1.453 cm (572 mils)	Zn- 1.686 cm (664 mils) ZnCa- 2.006 cm (790 mils)

AESAR, Seabrook, NH) was spot-welded onto a Ag mesh current collector (Exmet Corp., Bridgeport, CT, 5Ag54-0). The ZnCa electrode was of the same initial mass as a full-capacity Zn electrode. Because a 25 mol% $Ca(OH)_2$ (based on the mol% Zn and Ca in the uncycled electrode, not including inert materials) exhibited good cycle-life performance in Zn/NiOOH cells [5], this composition was selected for use in the ZnCa/AgO cells. The density of $Ca(OH)_2$ is 2.24 g/cm^3, which may be compared to 5.61 g/cm^3 for ZnO. Therefore the ZnCa electrodes occupied a greater volume and thus required more binder and led to a thicker negative electrode. The electrode was 0.067" thick and contained 92 wt% ZnO+$Ca(OH)_2$, 2 wt% PbO, 5 wt% PTFE and 1 wt% newsprint. The procedure for fabricating ZnCa electrodes was similar to that for zinc electrodes [5].

(3) Separator and wick: Each Ag electrode was wrapped with a layer of Pellon and Celgard separators, which were provided by BST company, and five layers of cellophane as the outer separator layers. The Pellon is used as a wick to keep the Ag electrodes wet with electrolyte and is a non-woven nylon material. The BST-group cells used one layer of Dexter paper (The Dexter Crop., Windsor Locks, CT, Grade 10) around the Zn electrode, and the paper was sealed with cellophane tape (3M Corp., St. Paul, MN). In the LBL-group cells, two layers of Celgard 3401 (Celanese Fibers Corp., Summitt, NJ) microporous polypropylene sheet were heat-sealed around the zinc electrode.

(4) Electrolyte preparation: Table II lists the compositions of the various electrolytes that were tested. In order to simplify comparisons among these electrolytes, all of them were constituted to have a similar ionic strength (I ~15-16). The standard electrolyte was 45 wt% KOH AnalaR grade solution (J.T. Baker Chemicals Co., Phillipsburg, NJ). The K_2CO_3 and H_3BO_3 were ACS reagent-grade chemicals (Fisher Scientific, NJ) and the KF and K_3PO_4 were Baker AnalaR grade chemicals. In order to avoid contamination by CO_2, 15 Mohm-cm or better

TABLE II : Electrolyte Compositions*

BST-cell group :	
Standard :	45% KOH, ZnO saturated
Alkaline-fluoride-carbonate :	34% KOH, 3.6% KF, 8.8% K_2CO_3, ZnO saturated
	17% KOH, 8% KF, 19% K_2CO_3, ZnO saturated
	25.2% KOH, 12.4% KF, 8.8% K_2CO_3, ZnO saturated
	25.6% KOH, 3.9% KF, 15.9% K_2CO_3, ZnO saturated
LBL-cell group :	
Standard :	45% KOH, ZnO saturated
Alkaline-fluoride :	37% KOH, 9% KF, ZnO saturated
Alkaline-carbonate :	38% KOH, 8% K_2CO_3, ZnO saturated
Alkaline-borate :	39% KOH, 5% K_3BO_3, ZnO saturated
Alkaline-phosphate :	39% KOH, 6% K_3PO_4, ZnO saturated

* The wt% shown in the table are the compositions before addition of ZnO to the electrolyte

deionized water was used. Following preparation of each solution, ZnO was added in sufficient quantity to saturate the electrolyte.

(5) Cell assembly: The cell pack (separator/electrode) assembly was designed for split-wrap [2] configuration. The positive electrodes were wrapped in pairs and the tube thus formed was folded at the center line so that two electrodes were enclosed in one bag and the negative electrodes were individually bagged with the bottoms sealed. The cell cases were made from polysulfone (for the BST-group cells) and from acrylic (for the LBL-group cells). In order to analyze the behavior of individual electrodes, a reference electrode was used for every cell except B1 and B2. A Hg/HgO electrode located in a separate reference compartment that was filled with the same electrolyte was used as the reference electrode. The cell pack was placed in a tightly fitting cell case, and each cell was filled with 20 ml of electrolyte. The rate at which the electrodes absorbed the electrolyte was slow because five layers of cellophane were used, and the cell pack was under pressure. The electrode soak time was about 5 days. The cell was vented and an Ascarite column was attached to prevent CO_2 from entering the cell.

(6) Cell cycling tests: Cells were cycled under controlled charge and discharge regimens using a combination of analog and digital equipment, which has been described in detail in Ref. [8]. All cells were tested at constant current. Prior to beginning regular cycle testing, two formation cycles were performed in order to render the cell active. The first formation cycle employed a 0.5-A charge to a 2.2-V cell cut-off voltage, followed by a 0.5-A discharge to a 1.1-V cut-off. The second formation cycle employed a 0.5-A charge to a 2.01-V cell cut-off voltage, followed by a 0.5-A discharge to a 1.1-V cell cut-off voltage. Standard cycle testing used 0.5-A charge current to a 2.01-V cell cut-off voltage and a 1.0-A discharge current to a 1.1-V cell cut-off voltage. An open-circuit period of 30 minutes was implemented at the end of each half-cycle.

(7) Analysis of cycled cells: After cells completed cycling, the Zn electrodes were examined to

determine extent of the shape charge, and each separator layer was analyzed for Ag content. Zinc electrode shape change was determined by analysis of x-ray photographs, which were obtained using a 60-KeV x-ray beam, and an exposure of 100 mAs. Scanning electron microscopy (SEM) was employed for qualitative analysis of the zinc electrode morphology. An AMR model 1000 SEM was used for this purpose. The Ag content of the separator was deteremined by Volhard methods [9]. Samples of the separators were cut from the electrodes. Each sample was cleaned several times with distilled water, and then placed in a 250-ml beaker with 25 ml of 42 wt% nitric acid. The beaker was heated for about 30 minutes to aid in the dissolution of the Ag from the separator sample. The resulting solutions were titrated with 0.1 N or 0.01 N ammonium thiocyanate (Baker AnalaR grade) using ferric ammonium sulfate (Fisher Scientific ACS grade) as an indicator. The initial yellow color changed to reddish-brown at the end point. The tensile strength of the cellophane separators was measured in order to determine the effect of electrolyte composition on separator tensile strength. Measurements were made using an Instron electro-hydraulic tensile tester model 1321.

RESULTS AND DISCUSSION

A total of 6 cells in the BST-cell group were subjected to cycle-life testing to evaluate standard electrolytes (as a baseline test for comparison purposes), and the alkaline-fluoride and alkaline-carbonate electrolytes listed in Table II. Two cells [designed B1 and B1(2)] contained standard electrolyte (45% KOH) and four cells [designed B-2 through B-5] contained 34 wt% KOH/3.6 wt%KF/8.8 wt% K_2CO_3, 25.6 wt% KOH/3.9 wt% KF/15.9 wt% K_2CO_3, 17 wt% KOH/8 wt% KF/19 wt% K_2CO_3, and 25.2 wt% KOH/12.4 wt% KF/8.8 wt% K_2CO_3, respectively. Five cells of the LBL-cell group were subjected to cycle-life testing to evaluate the standard and alkaline-fluoride, -carbonate, -borate, -phosphate electrolytes listed in Table II. These cells [designed L1 through L5] contained standard electrolyte (45%KOH), 37 wt% KOH/9 wt% KF, 38 wt% KOH/8% K_2CO_3, 39 wt% KOH/5 wt% K_2BO_3, and 39 wt% KOH/6 wt% K_3PO_4,

respectively. Two cells with ZnCa negative electrodes in the LBL-cell group [designed as C1 and C1(2)] were used to evaluate ZnCa electrode performance in standard 45%KOH electrolyte. The following results that show the cell capacity retention data in this work are based on the cell rated capacities, *i.e.* 5 Ah = 100% capacity, regardless of the initial (maximum) capacity exhibited by the cell. Cells B1 and L1 with standard electrolyte were used as base-line control cells in the BST-cell and LBL-cell group.

Figure 2 shows a plot of capacity *vs* cycle number for the BST-cell group. All of the cells had at least 98% coulombic efficiency for all standard cycles. However cells with additives in the electrolyte exhibited a lower capacity than the cell with standard 45 wt% KOH electrolyte. Increasing amounts of KF added to KOH electrolyte resulted in a lower capacity than that exhibited by the control cell B1. The capacity of Cell B1 reached its maximum value (~115%) after about 20 cycles, and the capacity of Cell B1 remained above 80% of its initial value until it dropped to 77% after 135 cycles, followed by a sharp drop to 19%. Figures 3 - 7 show cell voltage *vs* time plots for various cycles for Cells B1 - B5 and B1(2). The shape of the discharge curve consists of a declining portion during the first 1.5 - 2 hours of discharge followed by a flat plateau for the next time period, after which the cell voltage drops rapidly to the 1.1-V cell cut-off voltage (when the discharge capacity is nearly exhausted). The charge curve also shows two steps (plateaus) before the charge cut-off voltage (2.01 V) is reached, and the first plateau (the formation of Ag_2O) is shorter than the second one (the formation of AgO). The average charge voltage is about 1.88 V, and the average discharge voltage is about 1.53 V. The shapes of the discharge curves indicate that the Ag electrode was capacity-limiting throughout all of the test regimens. Also, cells with additives have a lower capacity, which can be attributed to the behavior of the Ag electrode in the presence of the modified electrolytes. Even though Cell B1 exhibits a higher capacity, the discharge plateau shows an unusual declining slope decline (see Fig. 3). Figure 8 shows coulombic efficiencies *vs* cycle number for Cells B1 and B2. The

coulombic efficiencies were at least 98% for all standard cycles. Open-circuit stand tests (to evaluate charge retention) for Cell B1 were conducted at cycles 46, 47, and 103 for 84, 87 and 73 hours, respectively. The cell maintained its normal coulombic efficiency (>98%) during these tests. However, the coulombic efficiency declined to about 92% after a 52-hour open-circuit test at cycle 125, and the coulombic efficiency fell below 25% after cycle 135. The lower coulombic efficiency at the end of cell life suggests that the failure of Cell B1 can be attributed to zinc dendrites (hard short). Cell B2 retained more than 82% of its initial capacity after 60 cycles, but its coulombic efficiency dropped to about 75% (see Fig. 8). Also, the charge voltage was "choppy" near the cut-off voltage (see Fig. 4). The choppy cell voltage suggests dendrite formation, and dendrite growth was indeed observed around the negative electrodes.

Figures 9 and 10 show the capacity and coulombic efficiency *vs* cycle number for Cells B1 and B1(2). Cell B1(2) was intended to replicate the long-lived and high-capacity "baseline" Cell B1. However, Cell B1(2) could not maintain high capacity (>95%) after 40 cycles, and dropped to 73% capacity at cycle 65. Obviously, Cell B1(2) exhibited a lower capacity than that of Cell B1, although both cells had similar coulombic efficiency (at least 98%, see Fig. 10).

Figure 11 shows capacity *vs* cycle number for Cells L1 - L5. Similar to the results with the BST-cell group, cells with different electrolyte additives (fluoride, carbonate, borate, and phosphate) showed generally lower capacities, especially those with fluoride and phosphate additives. Figures 12 - 16 show cell voltages and electrode potentials for the LBL-cell group. All cells exhibit the expected shapes of charge and discharge curves. However, the plots clearly show that the Ag electrode limits the capacity of all lower-capacity cells. This phenomenon can be attributed to the formation of inorganic salts at the Ag electrode (*eg* AgF or AgF_2, $AgPO_4$, *etc*) resulting in Ag active materials loss. The "baseline" Cell L1 reached 115 cycles and maintained 80% of its original capacity. Figures 17 and 18 show capacity and coulombic efficiency

vs cycle number for Cells L1 and C1. Both cells were filled with 45 wt% KOH electrolyte and employed the same separator system, and differed only in the composition of the Zn electrode. However, Cell C1 with $Ca(OH)_2$ in the zinc electrode showed higher capacity and longer cycle-life. Obviously, the additive $Ca(OH)_2$ has a positive effect in Zn/AgO cells. Both cells showed normal coulombic efficiencies (>98%). The total delivered capacity was 538 Ah for Cell L1 and 598 Ah for Cell C1 for the first 120 cycles, over which both of cells maintained >80% of rated capacity. This difference in performance can be attributed to the addition of $Ca(OH)_2$ to the Zn electrode, which results in the formation of an insoluble $Ca(OH)_2.2Zn(OH)_2.2H_2O$ complex (6), which lowers the concentration of soluble zincate species and causes somewhat different cell behavior. Especially at higher KOH concentration, the calcium-zincate decomposition rates are relatively fast (10).

Figure 19 shows cell voltage and electrode potentials for different cycles for Cell C1. The first charge plateau (the formation of Ag_2O) was longer than typical and became shorter with increasing cycle number. The unusually long first charge plateau results in higher capacity and lower average charge voltage. Also, the flat discharge plateau was longer than typical, and the average discharge voltage was lower. During the oxidation of Ag electrodes, the formation of Ag_2O and AgO films results in two charge plateaus, where the second charge plateau (the formation of AgO film) is longer than the first one (the formation of Ag_2O film). At moderate current densities, both processes are about 100% efficient (11). Therefore, the length of the plateaus is a function of the relative thicknesses of the oxide films. Generally, the thickness of the film depends on the current density, electrolyte concentration, and physical state of that electrode (12). The faster calcium-zincate decomposition rate [compared to the decomposition rate of $K_2Zn(OH)_4$] in higher KOH concentration electrolytes facilitates OH^- transport from the Zn electrode to the Ag electrode, and can thereby result in the longer first charge plateau (or thicker Ag_2O film). However, after a few cycles, the deposition of Ag on the separator may hinder OH^-

ion transport from the Zn to the Ag electrode. Also, active material loss in electrodes results in a shorter charge plateau and lower capacity. Open-circuit stand tests (to evaluate charge retention) for Cell C1 were conducted at cycles 59, 76 and 180 for 72, 48 and 58 hours, respectively. The cell maintained its normal coulombic efficiency (>98%) during these tests. Unlike Cell B1, Cell C1 did not exhibit dendrite problems, even after 180 cycles.

Cell C1(2) was intended to replicate the long-lived and high-capacity "base-line" Cell C1. Both cells had the same cell pack design, and differed only in the thickness of the respective cell cases. Cell C1(2) had a 0.040"-thicker cell case than Cell C1. Figure 20 shows the capacity *vs* cycle number plots for Cells C1 and C1(2). Both cells showed a similar maximum capacity of ~122% of the rated value between cycles 15 and 20. Because Cell C1(2) showed only 90% of rated capacity after its formation cycles, the capacity of Cell C1(2) was lower than that of Cell C1, however the the shapes of capacity curves were similar.

Figure 21 shows capacity *vs* cycle number for Cells B1, L1 and C1. All three cells were constructed in a similar manner, and the major difference among these cells is the composition and fabrication of the Zn electrodes. The Zn electrodes utilized in Cell B1 were made by BST, Inc. and LBL fabricated the Zn electrodes used in in Cells L1 and C1. $Ca(OH)_2$ was added to the Zn electrodes only in Cell C1, as described above. Also, one layer of Dexter paper was used around the Zn electrode in Cell B1, and two layers of Celgard 3401 were used in Cells L1 and C1. Dendrite problems were the cause of failure only in Cell B1 (after 136 cycles). Apparently, the separator Celgard 3401 has the beneficial effect of preventing dendrite growth in these cells. Cells B1 and C1 showed comparable total delivered capacity (~656 Ah) and Cell L1 exhibited a somewhat lower total delivered capacities (~601 Ah), after the cells completed 136 cycles before Cell B1 failed. Even though Cells B1 and C1 show comparable capacities, Cell C1 exhibited higher capacities early in life and a longer cycle life.

The Ag content of the separators was determined after the cells completed their cycling tests. Figures 22 - 27 show the Ag content of the separator system for different cells for various completed cycle numbers. All cells showed the highest Ag content at the first layer of cellophane adjacent to the Ag electrode. Cells B1 and C1, after completing 136 and 185 cycles, respectively, showed that Ag penetration became progressively smaller through one layer of Pellon wick, one layer of Celgard and three layers of cellophane (see Figs. 22 and 27). Cells B2 and B3, which had lower KOH concentration, showed higher Ag contents on the separator layers, compared to Cell B1 (see Figs. 23 and 24). This observation can be attributed to a higher Ag solubility and greater separator degradation rate for Cells B2 and B3. Table III shows the results of the tensile-strength test of cellophanes in different electrolytes for different periods of time. These results show that tensile strength decreased with lower KOH concentrations.

TABLE III : Tensile Strength* of Cellophane

Sample Condition	Breaking Load (lbs.)
dry	5.3
wet	0.72
Hydrolysis conditions --- 45% KOH + satd. ZnO & AgO at 90 °C	
24 hrs.	0.48
48 hrs.	0.23
72 hrs.	0.07
Hydrolysis conditions --- 39% KOH + 5% K_3BO_3 + satd. ZnO & AgO at 90 °C	
24 hrs	0.41
48 hrs	0.1
Hydrolysis conditions --- 38% KOH + 8% K_2CO_3 + satd. ZnO & AgO at 90 °C	
24 hrs	0.38

* Loading Speed = 4 in./min.
Loading Sample = 4" x 3/8"

Figure 28 shows x-ray images of uncycled zinc and zinc-calcium electrodes. As can be seen, there is a uniform distribution of active materials over the Ag mesh current collectors. X-ray images of numerous zinc electrodes were recorded to assess the rate and extent of zinc material redistribution (shape change) that accompanied cell cycling. Figures 29 and 30 show x-ray images of Cells B1, L1, C1, C1(2), L3, and L4 after the cells had completed the numbers of cycles indicated in the figure caption. All cells were examined in the discharged state, *i.e.* after discharging each cell to the 1.1-V cut-off voltage. Both Figures 29 and 30 show, from left to right, zinc electrode #1 (a zinc electrode nearest to the cell container), zinc electrode #2, zinc electrode #3 and zinc electrode #4 (at the center of the cell pack). The cell shape-change patterns were symmetrical, *i.e.* the shape change pattern for zinc electrode #7 was similar to that of zinc electrode #1, the shape-change pattern of zinc electrode #6 was similar to that of zinc electrode #2, and so on. Cell B1 showed a modest extent of shape change after attaining 136 cycles. The LBL-cell group [L1, C1, C1(2), L3, and L4] showed more-extensive shape change, and the shape-change patterns were rather similar to one another. Three types of morphology can be easily distinguished in the electrodes of the LBL-group cells: (*i*) a dense, compact zinc area at the bottoms of the electrodes, (*ii*) "islands" of zinc, and (*iii*) areas of nearly bare current collector with a slight residual amount of zinc. The outermost zinc electrode (zinc electrode #1), which started cycling with half the capacity of its neighbors, exhibited mostly areas of nearly bare current collector and areas of dense, compact zinc. The island areas were more commonly found in the inner zinc electrodes (*i.e.* #2 through #6).

Other investigators [3 - 5] have shown that additions of calcium can reduce the rate and extent of zinc electrode shape change, particularly in electrolytes of low-to-moderate KOH concentration, because of the formation of a calcium-zincate complex. Cell C1 exhibited extensive zinc electrode shape change, which leads one to suspect that the formation of the calcium-zinc complex was inhibited by the high (45 wt%) KOH concentration [this turns out not to be the

case - see below]. It appears to be more likely that the use of Dexter paper around the zinc electrodes in the BST cells inhibits the rate and extent of shape change, at least in 45 wt% KOH electrolyte (see Fig. 29), compared to the LBL cells which employed Celgard separator next to the zinc electrodes. Different types of Ag-electrode current collectors were used in the LBL-group and BST-group cells (mesh and sheet, respectively), however it is less likely that this difference is the root cause of the dramatically different shape change patterns.

The three distinct areas of the various zinc electrode samples (nearly bare current collector, island, and dense areas) harvested from Cells B1, L1 and C1 were examined microscopically using a SEM. This examination permits an assessment of the physical and chemical variations over microscopic areas of the electrodes. Figures 31-33 show the morphologies of selected areas in zinc electrodes from Cells B1, L1 and C1, respectively. In Cell B1 (see Fig. 31a) the uppermost area of the electrode (mainly bare current collector) exhibited needle-like metallic Zn on the surface, which led the formation and growth of Zn dendrites. The lower area of the electrode (Fig. 31b) contained typical porous zinc/zinc oxide material. In Cell L1 (Fig. 32), the island area contained porous zinc/zinc oxide material, and the bare current collector and dense areas contained very compact material (Figs. 32a and 32c), however some of the material in these areas has a porosity similar to that of the island area. In Cell C1 (Fig. 33), all three areas exhibited crystals typical of the calcium zincate complex. In particular, the island area (Fig. 33b) contained large amounts of these diamond-shape crystals. The bare current collector and dense areas (Figs. 33a and 33c) contained fewer diamond-shaped crystals, and in the dense area hexagonal crystals were found. Obviously, the morphology of calcium-zinc electrodes differs dramatically from that of the typical zinc electrode, and the use of 45 wt% KOH electrolyte does not prevent the formation of calcium-zincate crystals. The good cycle-life performance of Cell C1 may be attributed the formation of the calcium-zinc complex, however the great extent of shape change suggests that even better performance could be realized, perhaps

by improving the wetting characteristics of the electrode.

Table IV lists cycle-life performance data for the three groups of 5-Ah Zn/AgO cells that were cycled. Included in this table are values of the capacity loss rate (expressed as %/cycle, based on the initial cell capacity) and the average delivered capacity per cycle, both based on the cell performance before its capacity dropped to 4.0 Ah. These "figures of merit" illustrate the superior cycle-life performance of the calcium-containing Zn/AgO cells.

TABLE IV

Cycle-Life Performance Data for Representative Groups of 5.0-Ah Zn/AgO Cells

Cell*	Electrolyte**	Total # Cycles Completed***	Final % Cap. *(% rated cap.)*	# Cycles *(Before cells reached 80% rated capacity)*	% Cap. Loss/Cycle+ *(Before cells reached 80% rated capacity)*	Avg. Ah/Cycle *(Before cells reached 80% rated capacity)*
BST-Group						
B1	$45OH^-$	136	19	134	0.19	4.85
B1(2)	$45OH^-$	65	73	59	0.47	4.79
B2	$34OH^-/3.6F^-/8.8CO_3^{-2}$	97	71	44	0.3	4.39
B3	$25.6OH^-/3.9F^-/15.9CO_3^{-2}$	70	62	29	0.63	4.17
B4	$25.2OH^-/12.4F^-/8.8CO_3^{-2}$	58	63	6	1.13	4.22
B5	$17OH^-/8F^-/19CO_3^{-2}$	5	65	0	-	-
LBL-Group (Zn)						
L1	$45OH^-$	144	75	114	0.26	4.51
L2	$37OH^-/9F^-$	45	60	10	0.29	4.30
L3	$38OH^-/8CO_3^{-2}$	151	78	60	0.38	4.30
L4	$39OH^-/5BO_3^{-3}$	94	77	53	0.52	4.34
L5	$39OH^-/6PO_4^{-3}$	21	69	0	-	-
LBL-Group (ZnCa)						
C1	$45OH^-$	185	56	124	0.24	4.95
C1(2)	$45OH^-$	118	75	101	0.12	4.89

*** separator system : BST-Group - / dexter // 5*cp / cg / pellon / +**
LBL-Group - / 2 * cg // 5*cp / cg / pellon / +

**** anions identified common K^+ ion, all numbers in wt%.**

***** failure mode : B1 - short; other cells - capacity loss.**

+ calculated based on the cell capacity at the first cycle.

CONCLUSIONS

1. The ability of reduced-zinc solubility electrolytes, prepared by adding F^-, CO_3^{2-}, BO_3^{3-} and PO_4^{3-} to KOH electrolyte, to extend the cycle life of Zn/AgO cells was examined. It would appear that all of the anion additives to KOH electrolytes result in lower capacities. Lower capacities can be attributed to poor Ag electrode behavior, which could be due to the formation of inorganic salts, *e.g.* AgF, AgF_2, Ag_2CO_3, Ag_2BO_3 and Ag_3PO_4, that cause active materials loss.

2. The calcium-containing zinc electrode was found to significantly improve the performance of the Zn/AgO cell by promoting higher capacities, especially over the initial 20 cycles. The higher capacities can be attributed to the formation of a calcium-zincate complex, crystals of which were found in the cycled zinc electrodes. This result bears further investigation.

3. In the analysis of the silver content of the separator, results showed that the Ag content became progressively smaller through a single layer of Pellon and Celgard and three layers of cellophane. Cellophane was a good material to prevent Ag penetration. The results of separator tensile strength measurements showed that the tensile strength of cellophane decreased with lower KOH concentration.

4. Because $Ca(OH)_2$ is a beneficial additive to the Zn electrode in Zn/AgO cells, it is suggested that further research focus on investigations of ZnCa/AgO cells to better understand the mechanism whereby the capacity improvements are realized, the development of ZnCa/AgO cells with improved wetting characteristics, the fabrication of sealed ZnCa/AgO cells, and characterization of large ZnCa/AgO cells.

ACKNOWLEDGMENTS

BST, Inc. provided several Zn/AgO cells, electrodes and cell parts. These materials were indispensable for the initiation of our experimental program, and for providing comparisons to LBL-fabricated cells. The authors wish to thank BST for providing these useful materials. The experimental and analytic help provided by Mr. Thomas Adler and Dr. Kathryn Striebel is gratefully acknowledged.

This work was supported by the Defense Advanced Research Projects Agency, Undersea Warfare Office, Submarine Technology Program, under ARPA Order Number MIPR N0002490MP70004, through the U.S. Department of Energy under Contract No. DE-AC01-76SF00098.

REFERENCES

1. D. Linden, in *Handbook of Batteries & Fuel Cells*, McGraw-Hill, Inc., New York, 1984.
2. A. Himy, in *Silver-Zinc Battery - Phenomena and Design Principles*, Vantage Press, New York, 1986.
3. F.R. McLarnon and E.J. Cairns, *J. Electrochem. Soc.*, **138**, 645 (1991).
4. E.G. Gagnon, *J. Electrochem. Soc.*, **133**, 1989 (1986).
5. R. Jain, F.R. McLarnon and E.J. Cairns, Lawrence Berkeley Laboratory Report No. LBL-25332, (1989).
6. E.G. Gagnon and R.A. Sharma, J. Electrochem. Soc., **133**, 2215 (1986)
7. J.T. Nichols, F.R. McLarnon and E.J. Cairns, Lawrence Berkeley Laboratory Report No. 17397 (1983).
8. M.H. Katz, J.T. Nichols, F.R. McLarnon, and E.J. Cairns, *J. Power Sources*, **10**, 149 (1983).
9. D.A. Skoog, D.M. West and F.J. Holler, in *Fundamentals of Analytical Chemistry*, Saunders College Publishing, (1988).
10. Y.-M. Wang, *J. Electrochem. Soc.*, **137**, 2800 (1990).
11. T.P. Dirkse, *J. Electrochem. Soc.*, **106**, 453 (1959).
12. A. Fleicher and J.J. Lander (eds.), in *Zinc-Silver Oxide Batteries*, p.136, John Wiley & Sons, Inc., 1971.

APPENDIX : Design Calculations for the Zn/AgO Cell

Desired Capacity = 5 Ah
Cycle Life : > 40 cycles @ 100% DOD
Discharge Rate = C/5 = 1 Amp
Electrode Size : 1.75" x 1.4" (4.4 cm x 3.6 cm)
Cycling Methode = CC
Cell Pack = 6 plates of positive electrodes and 7 plates of negative electrodes;
outside plates are negative (- / sep./ + / sep./ - / sep./ + / sep./ - / ...)

********** **Calculations** **********

Practical utilization of Ag = 3 g/Ah (1.3 x theoretical)
Total mass of Ag = Mag = 3 (g/Ah) x 5 (Ah) = 15 g-Ag
Let : K = Mzn/Mag = 1.15 (cycle life (> 40 cycles) required)
Total mass of Zn = Mzn = 15 (g) x 1.15 = 17.25 g-Zn (2.83 x theoretical)
Ag loading for each Ag plate = Mag/6 = 2.5 g-Ag
Zn loading for each Zn plate = Mzn/6 = 2.87 g-Zn
Assume equivalent thickness of current collector = 1 mil
Let : dag = 4.5 (g-Ag/cm^3) and dzn = 1.54 (g-Zn/cm^3)
P = thickness of Ag plate
N = thickness of Zn plate
2.5 (g-Ag/plate) = 15.8 (cm^2/plate) x (P - 0.00254) (cm) x 4.5 (g-Ag/cm^3)
2.87 (g-Zn/plate) = 15.8 (cm^2/plate) x (P - 0.00254) (cm) x 1.54 (g-Zn/cm^3)
Then, P = 0.0377 cm = 15 mils;
N = 0.1207 cm = 48 mils

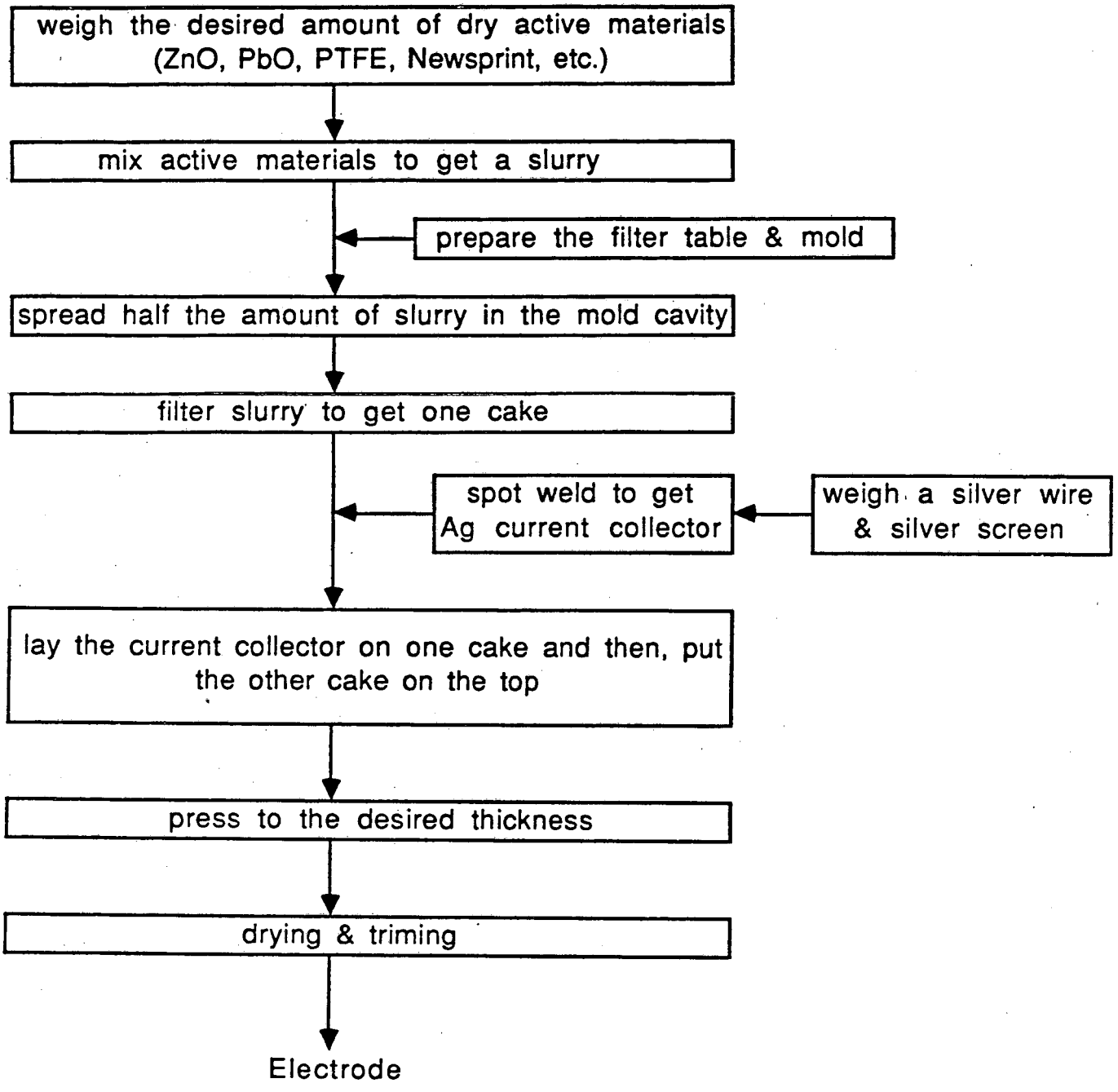

Figure 1 : Flow Chart for Making Zinc Electrodes for Zn/AgO Cells

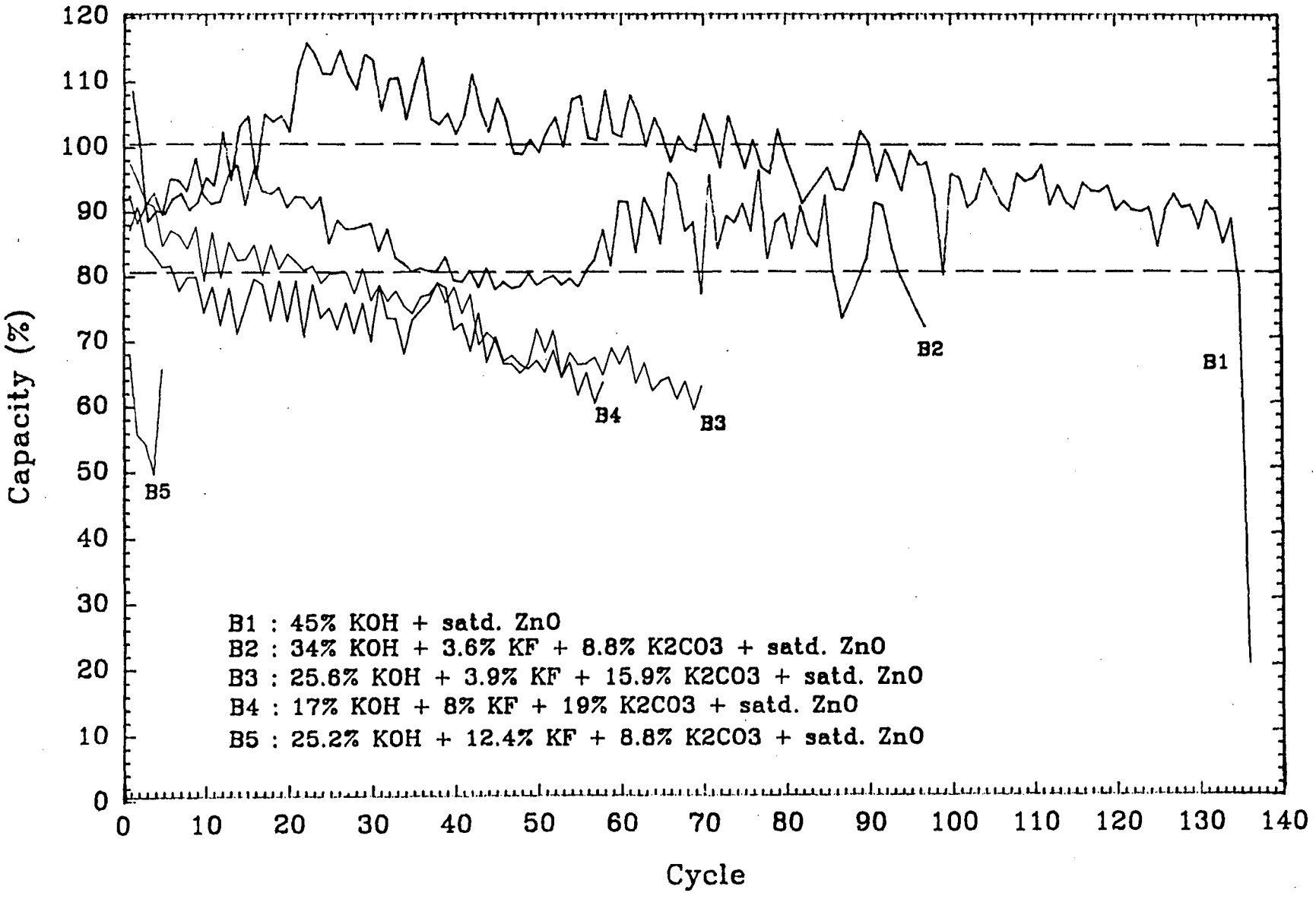

Figure 2 : capacity vs. cycle number for BST-cell group

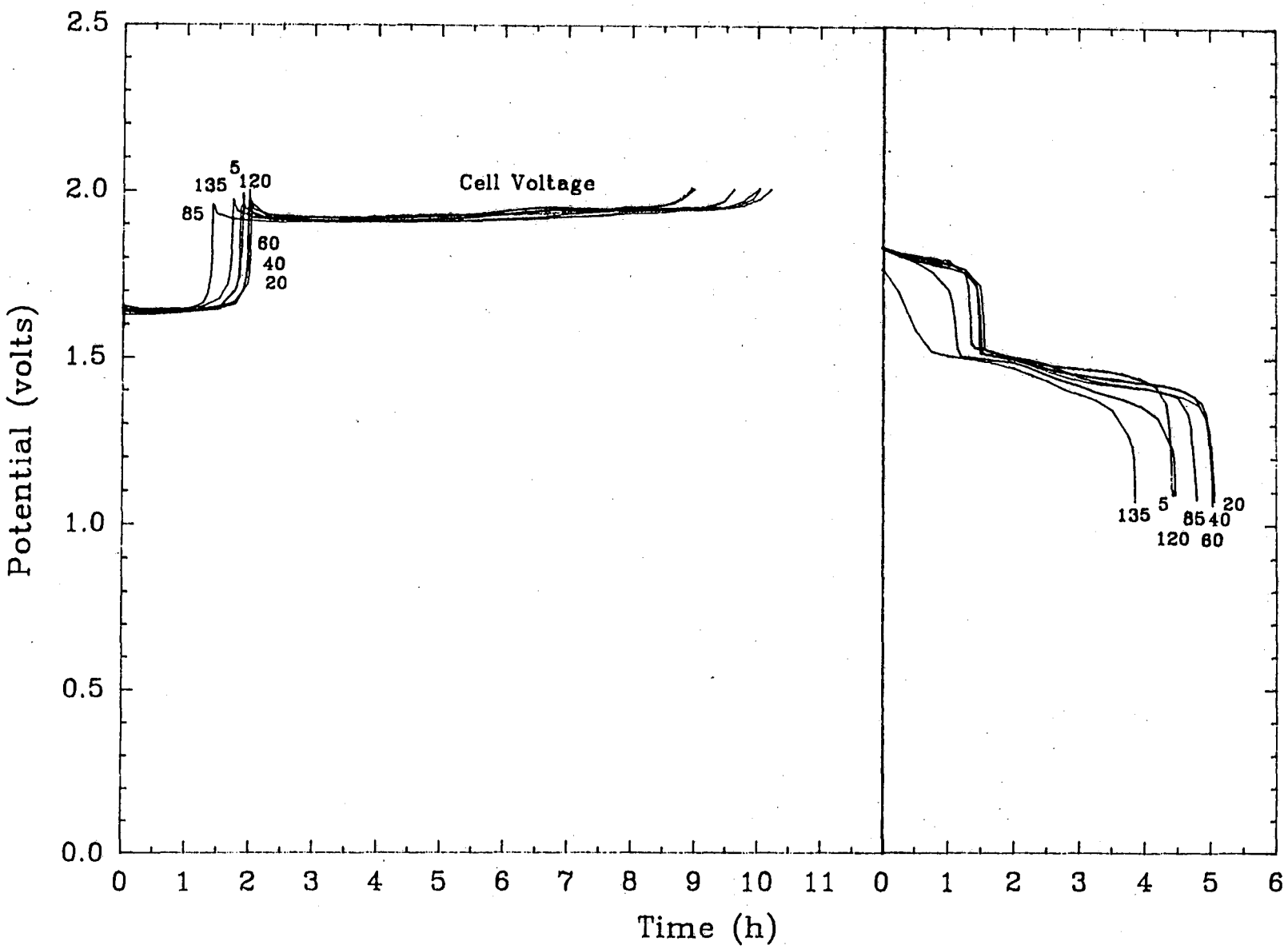

Figure 3 : cell voltage at different cycles for cell B1

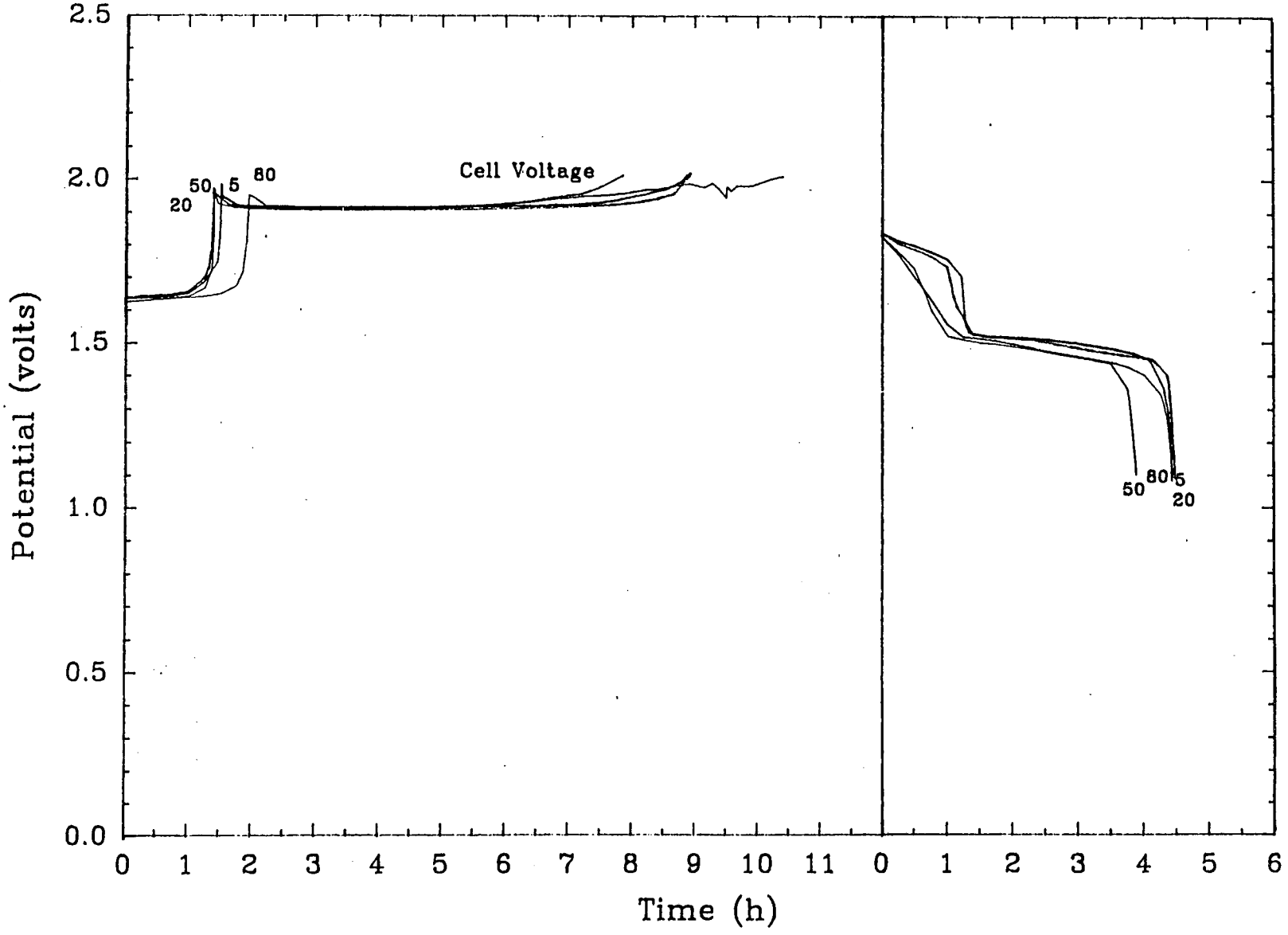

Figure 4 : cell voltage at different cycles for cell B2

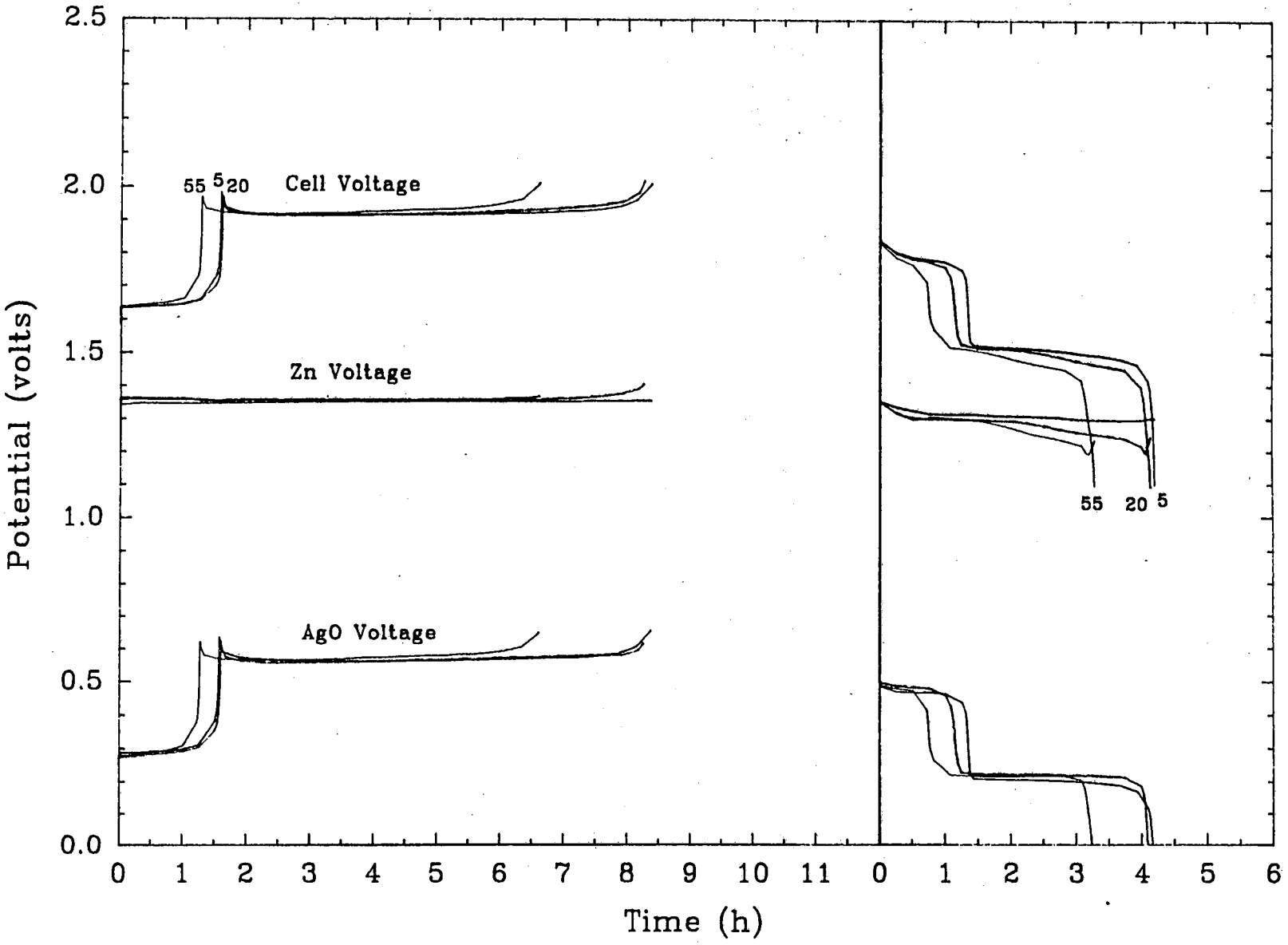

Figure 5 : cell voltage and reference voltages at different cycles for cell B3

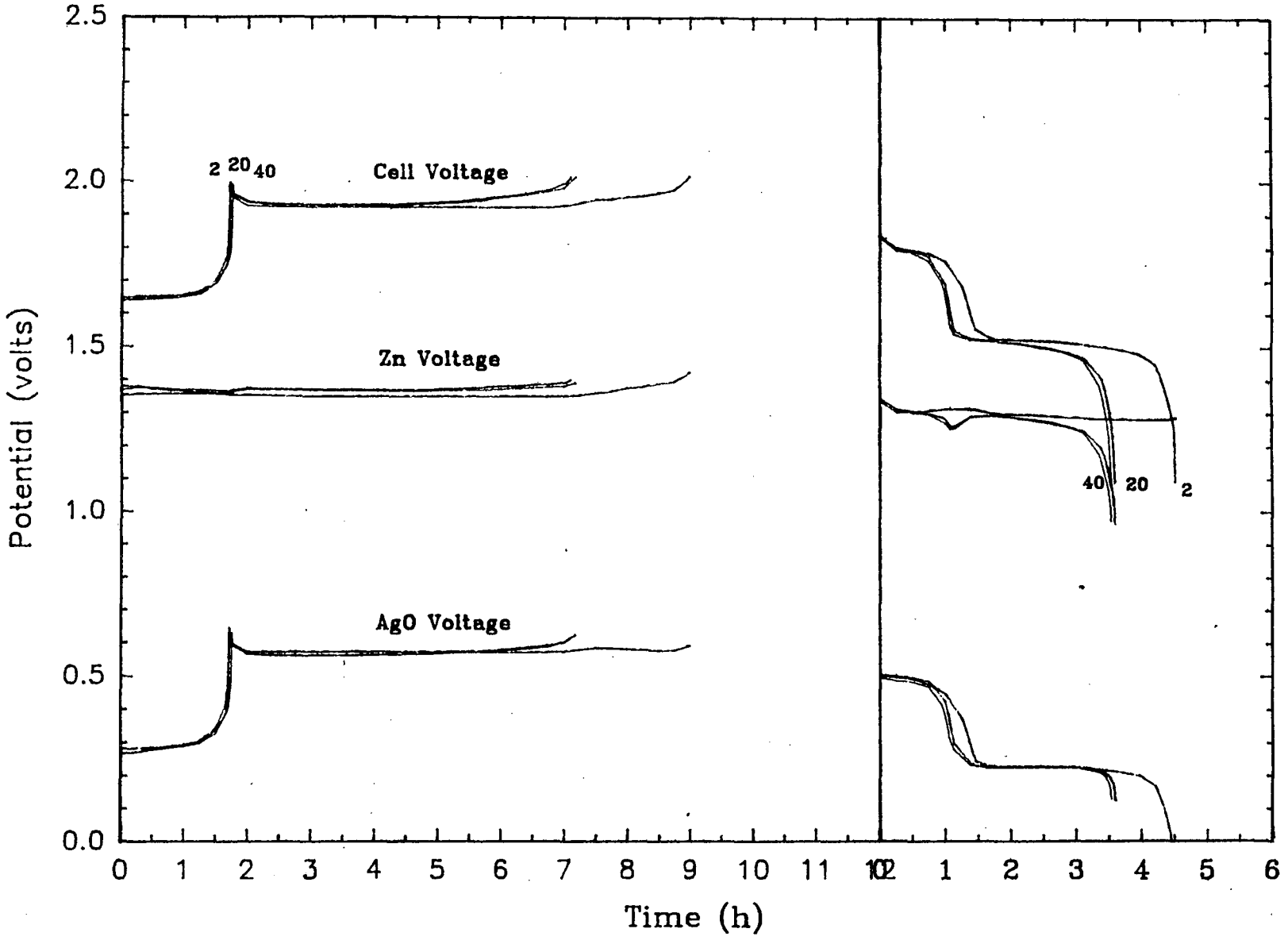

Figure 6 : cell voltage and reference voltages at different cycles for cell B4

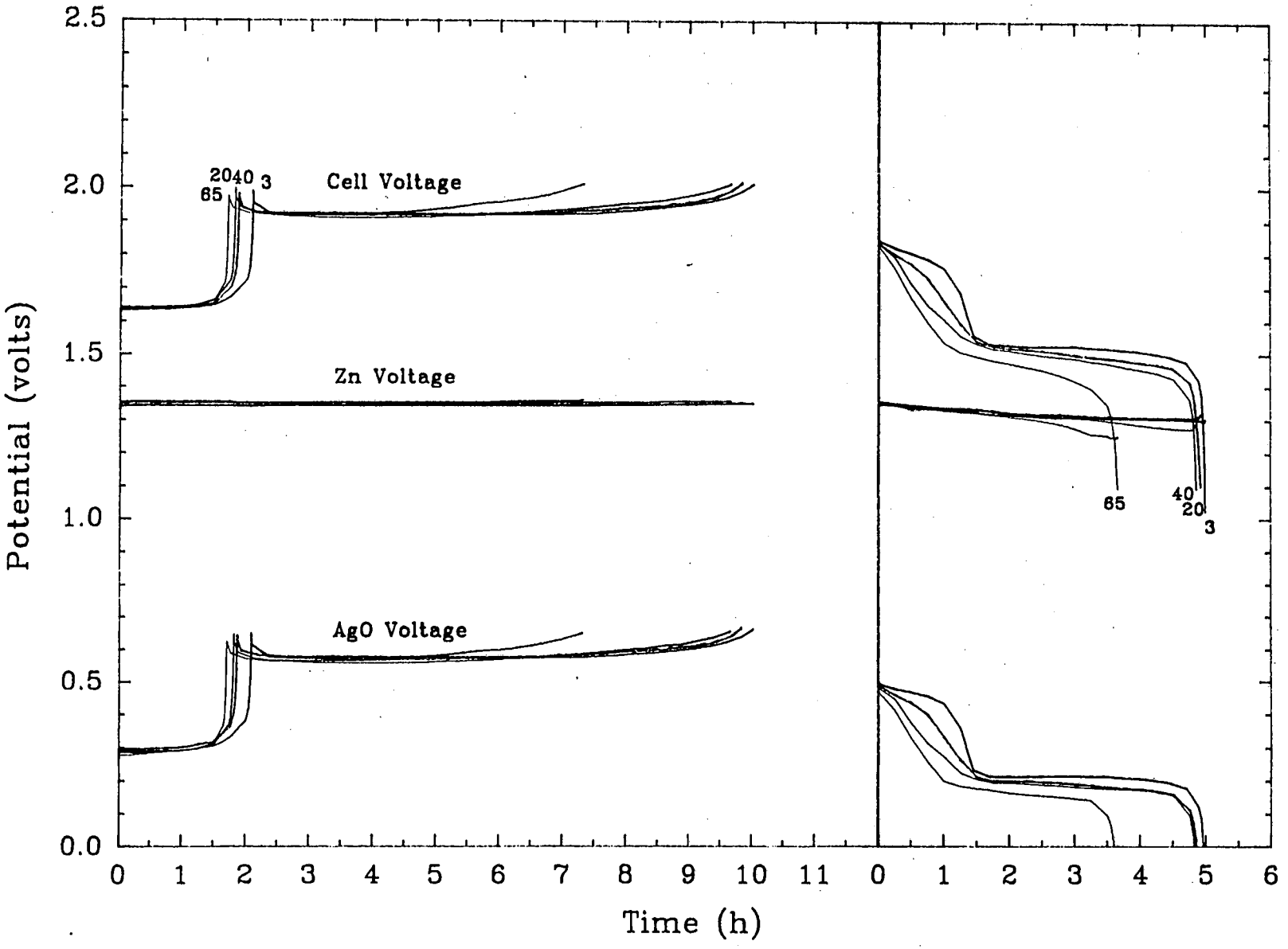

Figure 7 : cell voltage and reference voltages at different cycles for cell B1(2)

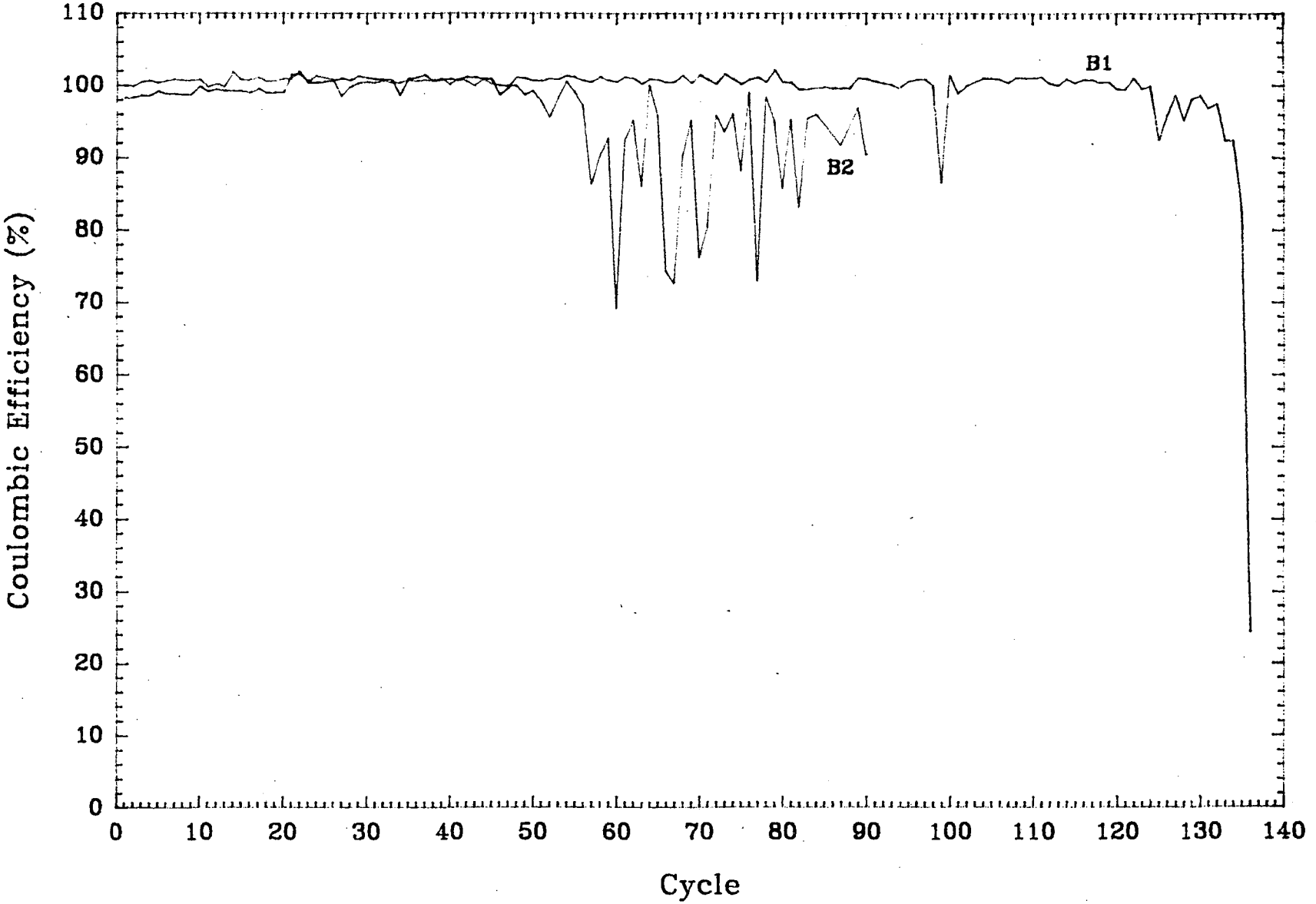

Figure 8 : coulombic efficiency vs. cycle number for cells B1 and B2

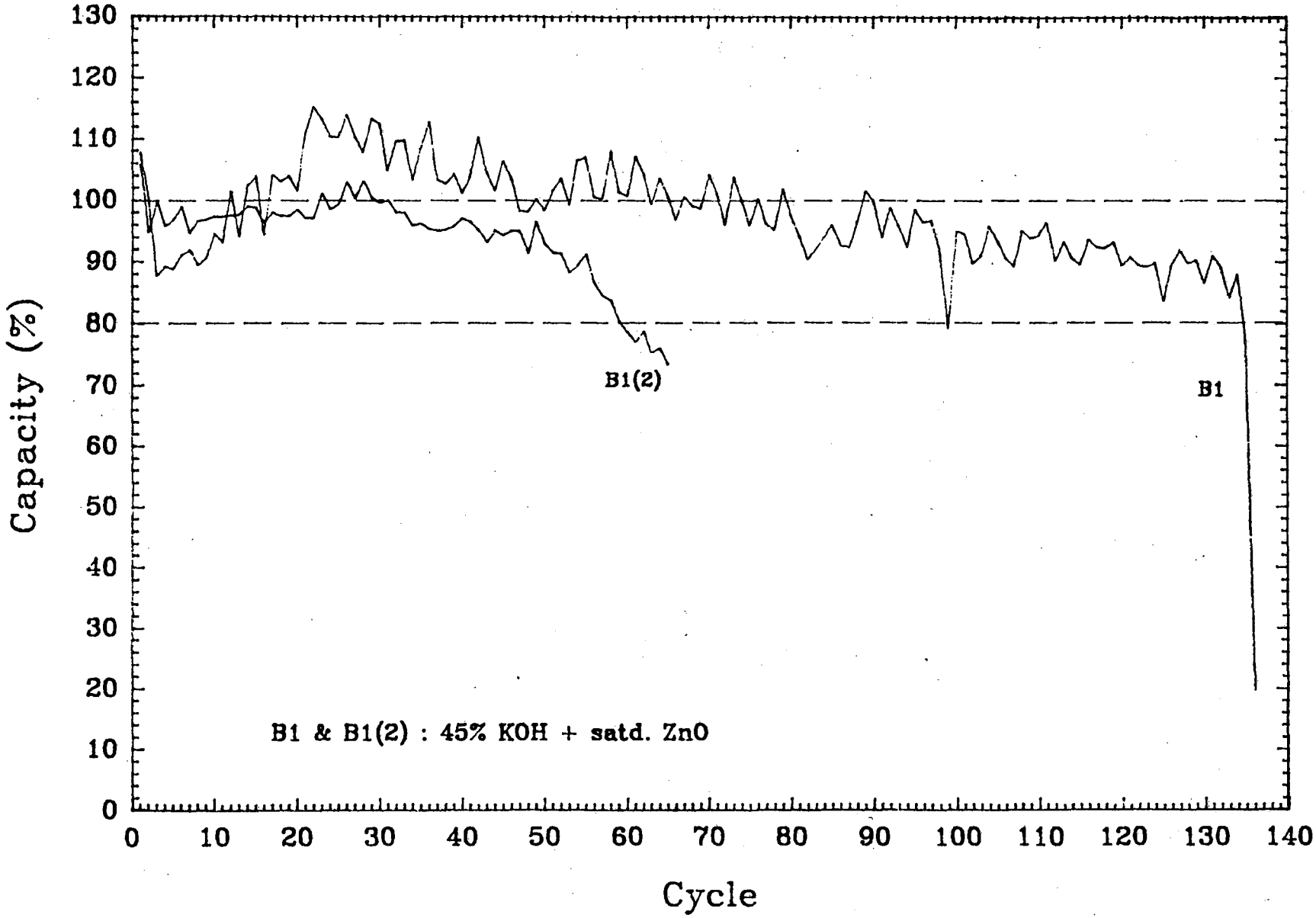

Figure 9 : capacity vs. cycle number for cells B1 and B1(2)

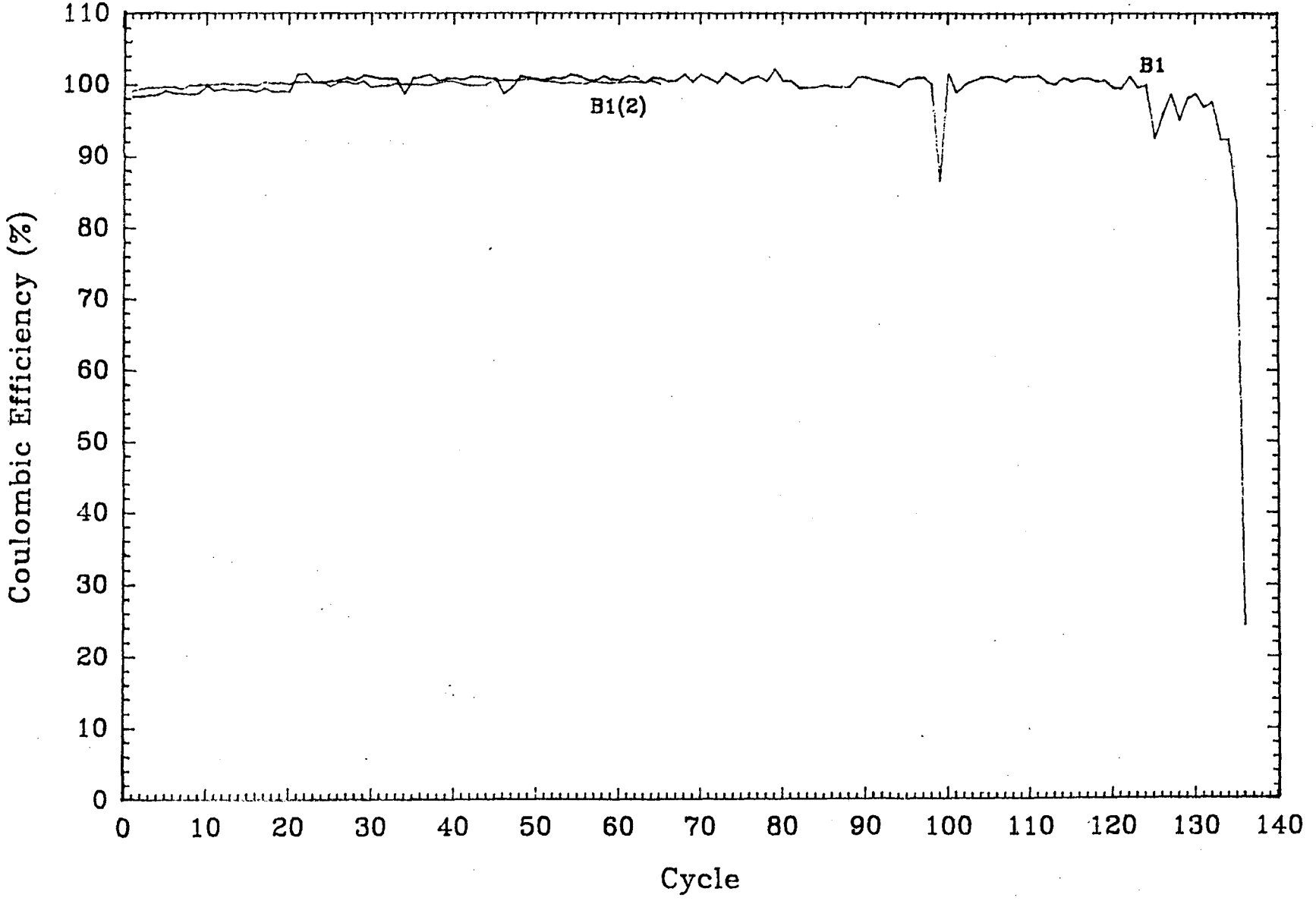

Figure 10 : coulombic efficiency vs. cycle number for cells B1 and B1(2)

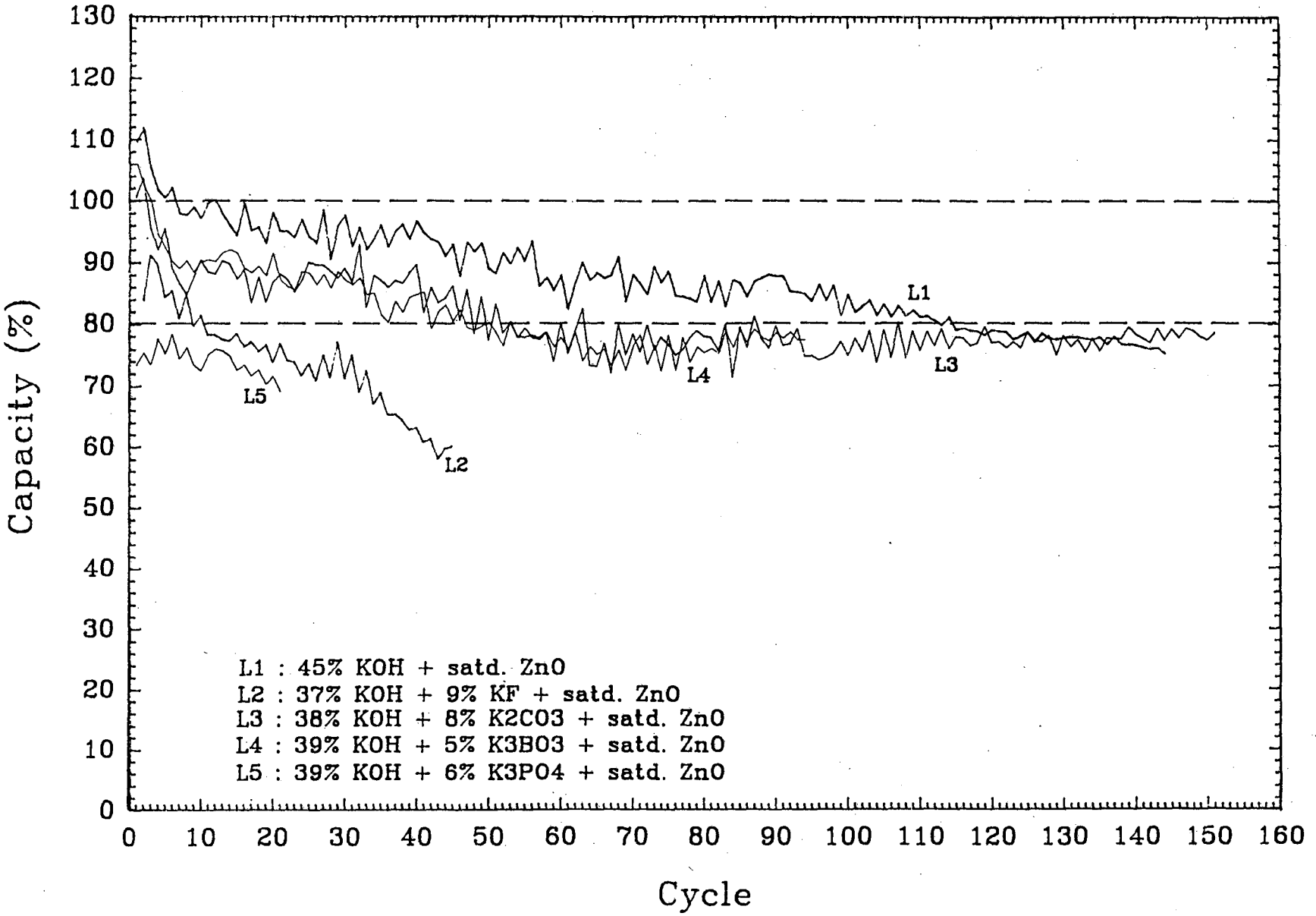

Figure 11 : capacity vs. cycle number for LBL–cell group

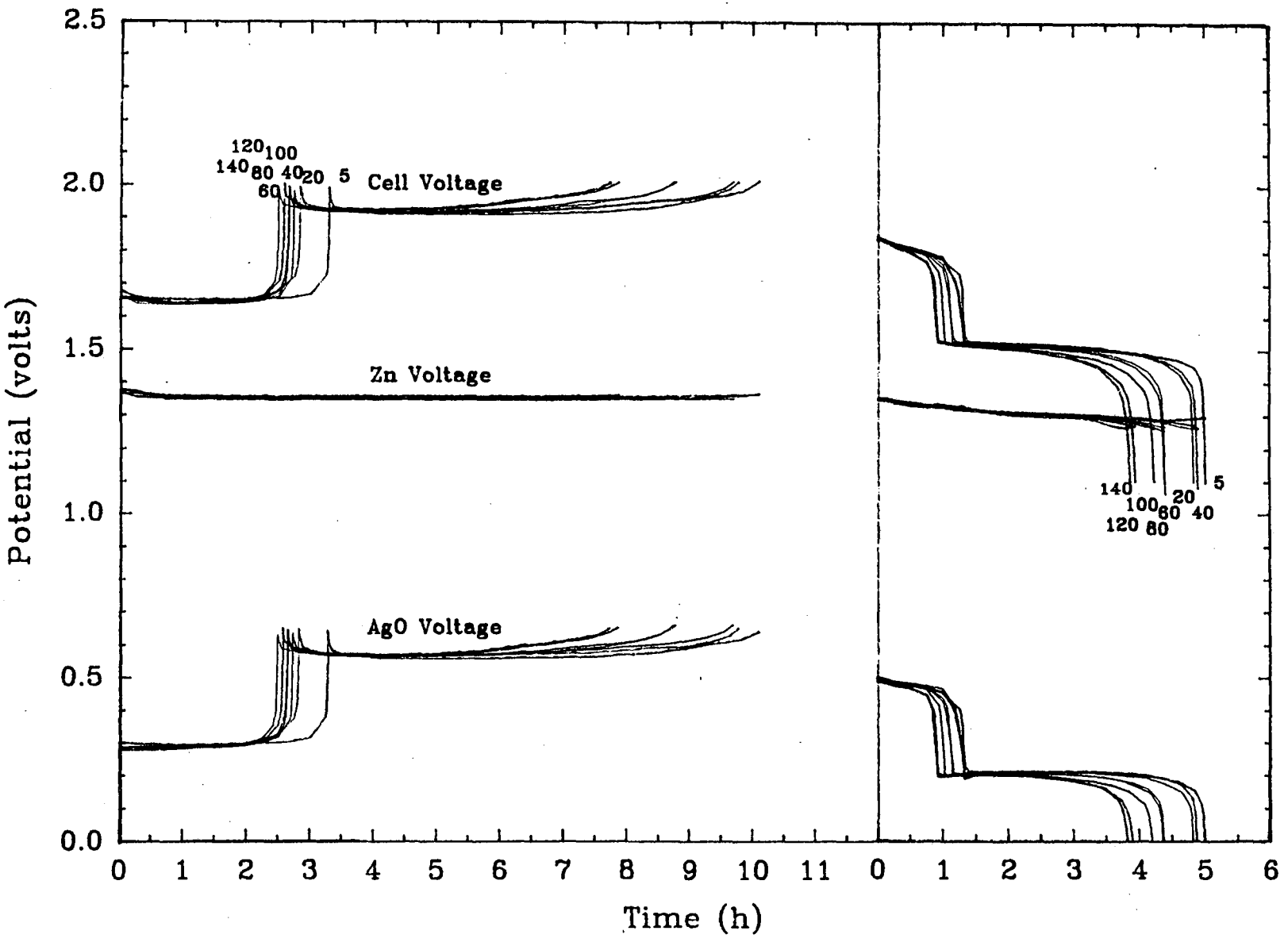

Figure 12 : cell voltage and reference voltages at different cycles for cell L1

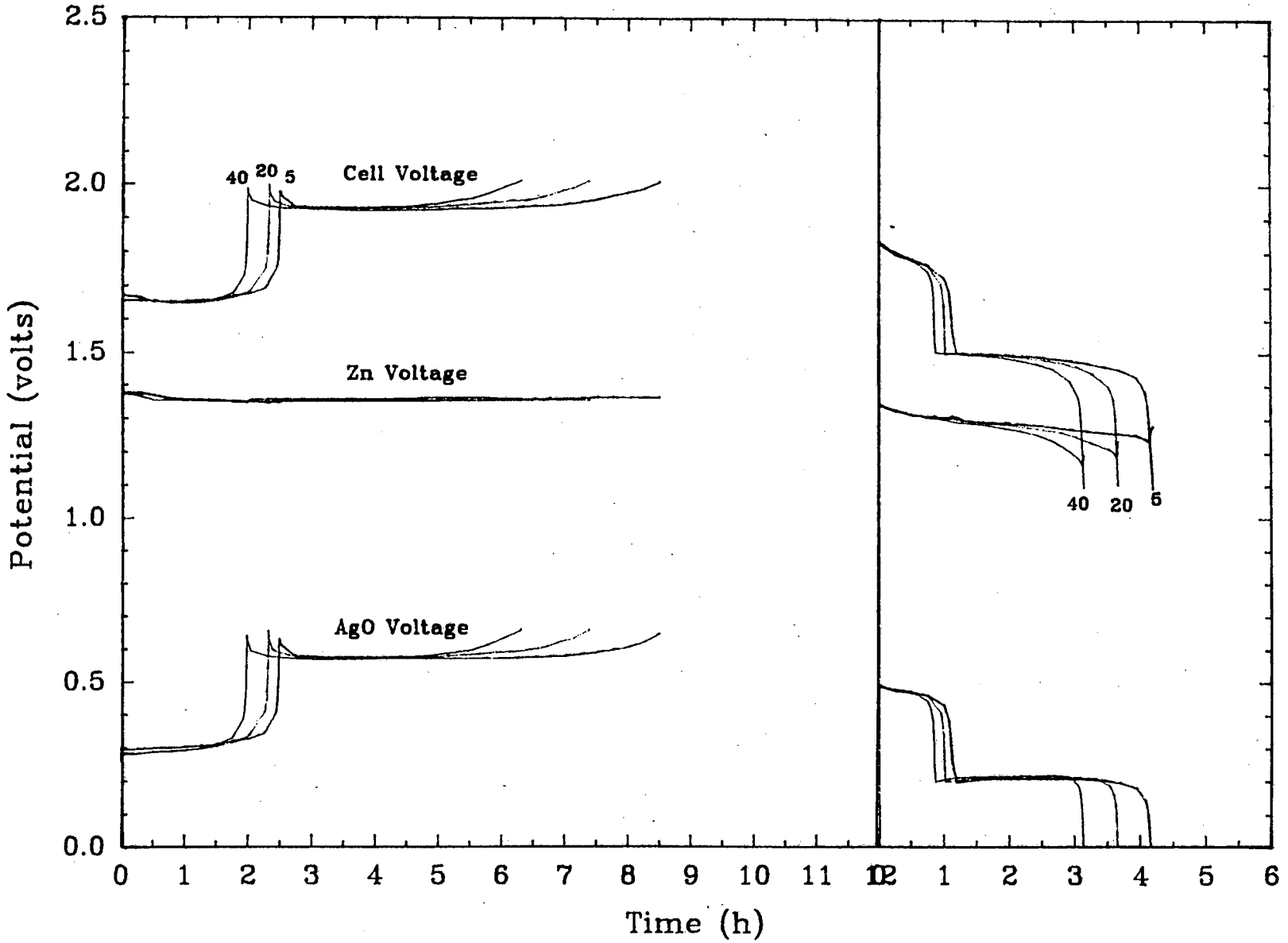

Figure 13 : cell voltage and reference voltages at different cycles for cell L2

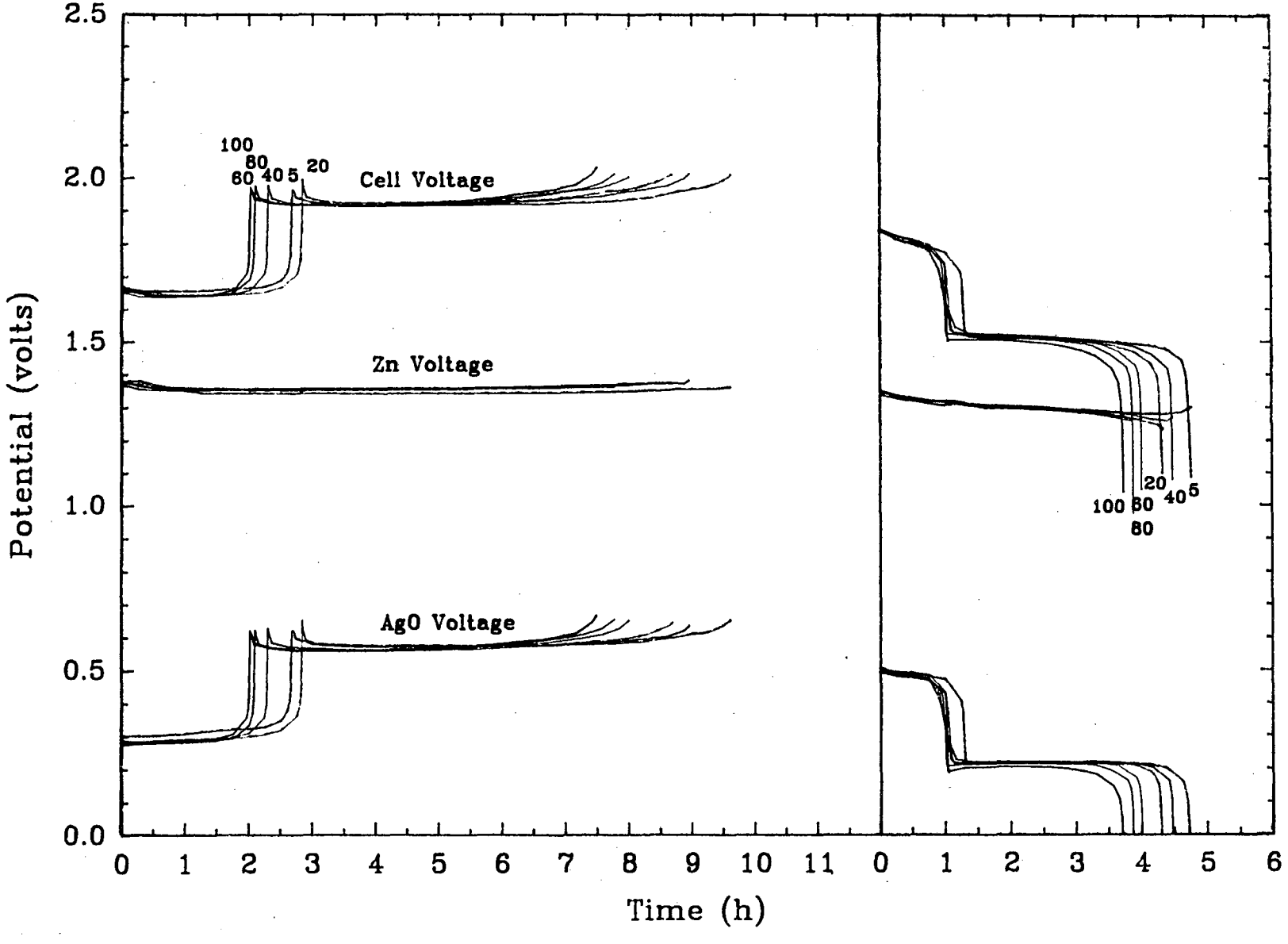

Figure 14 : cell voltage and reference voltages at different cycles for cell L3

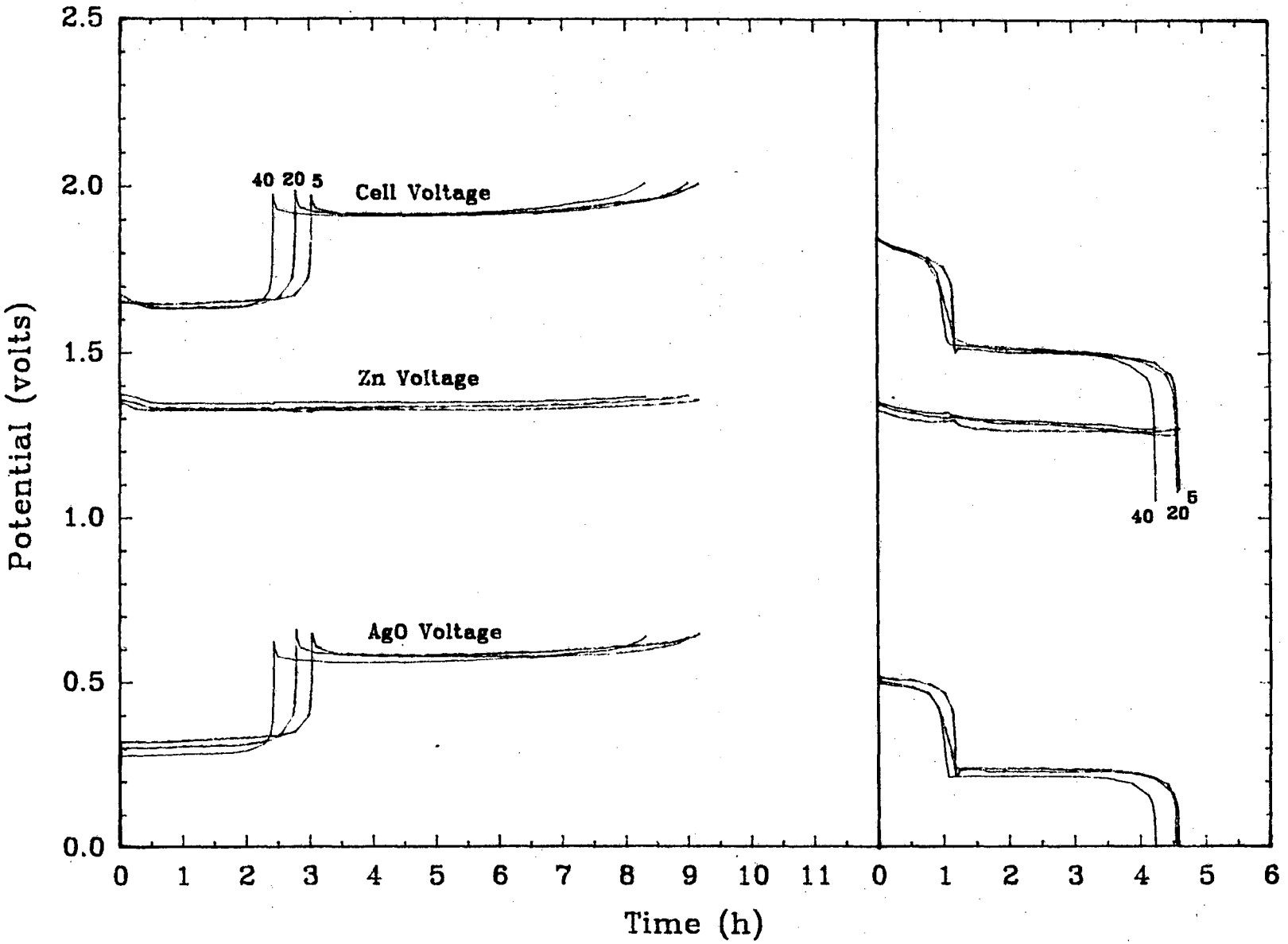

Figure 15 : cell voltage and reference voltages at different cycles for cell L4

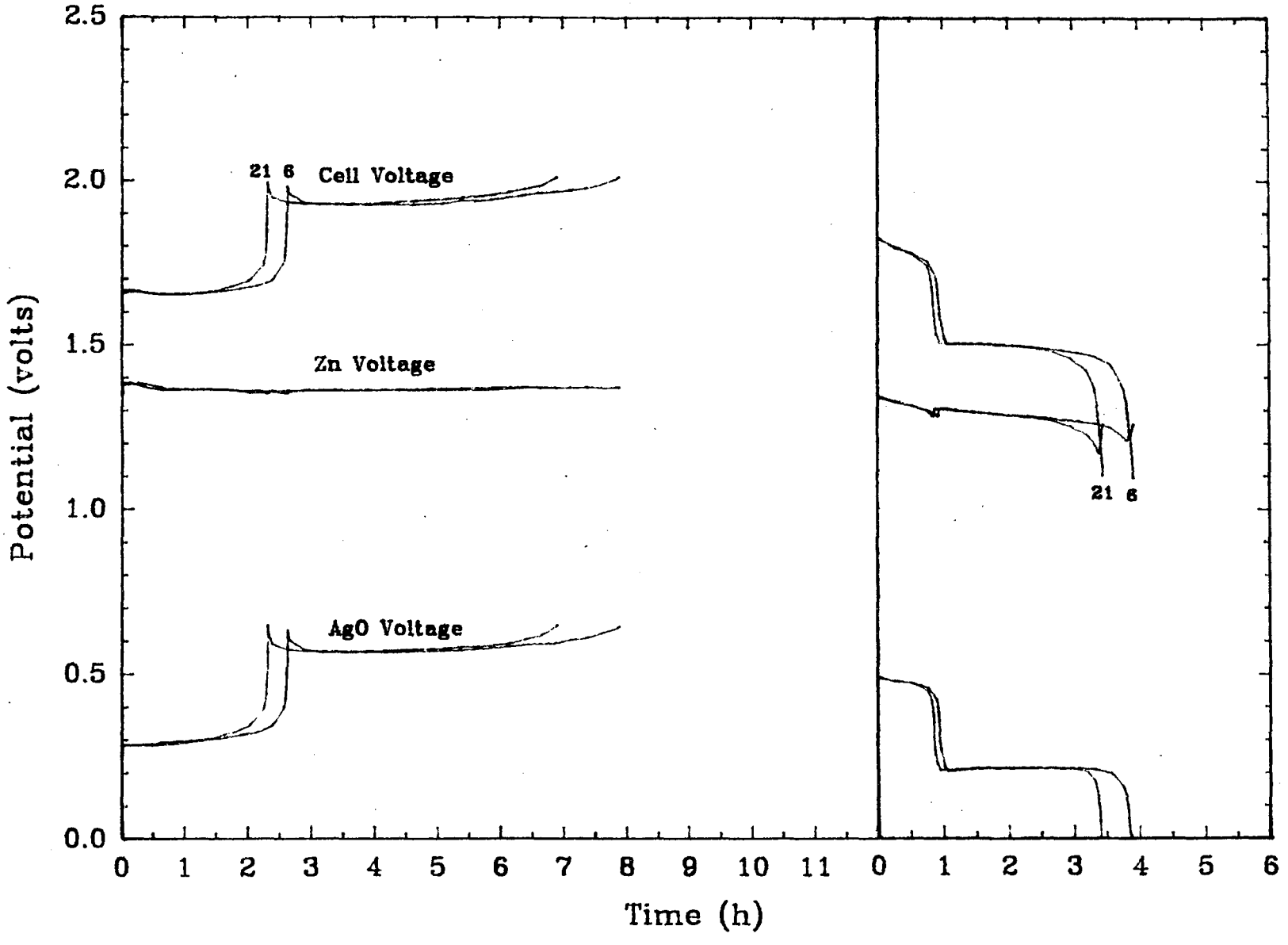

Figure 16 : cell voltage and reference voltages at different cycles for cell L5

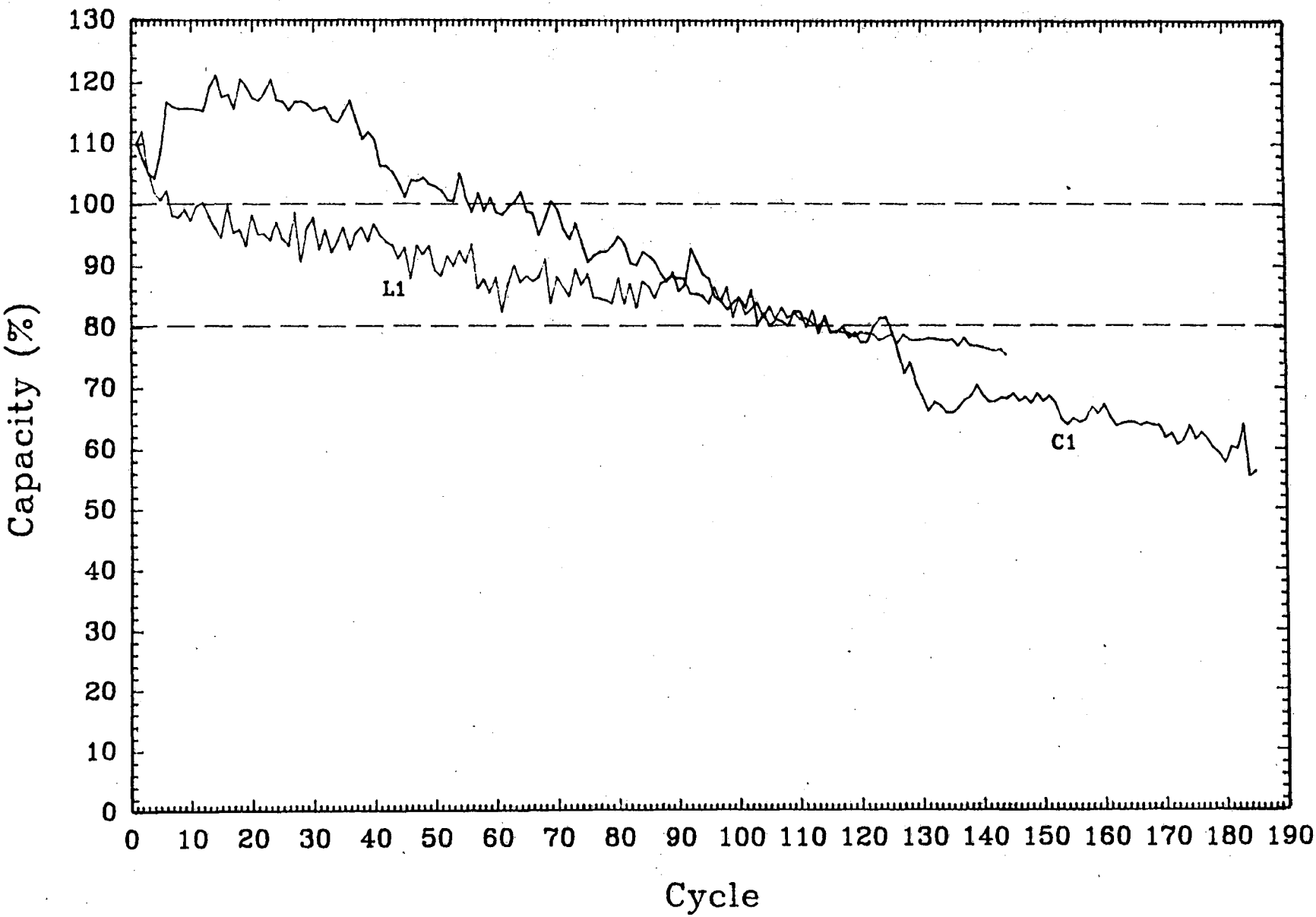

Figure 17 : capacity vs. cycle number for cells L1 and C1

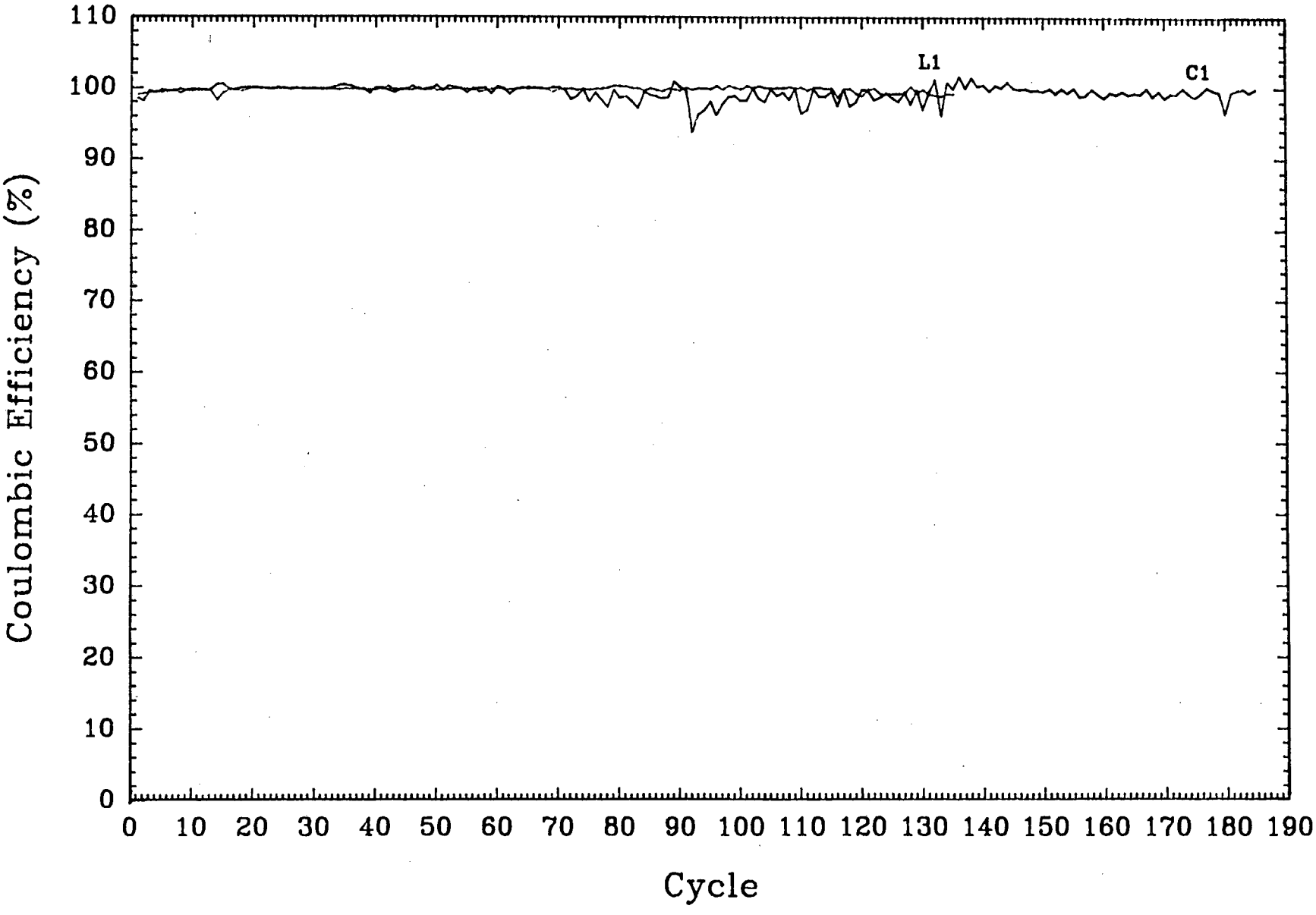

Figure 18 : coulombic efficiency vs. cycle number for cells L1 and C1

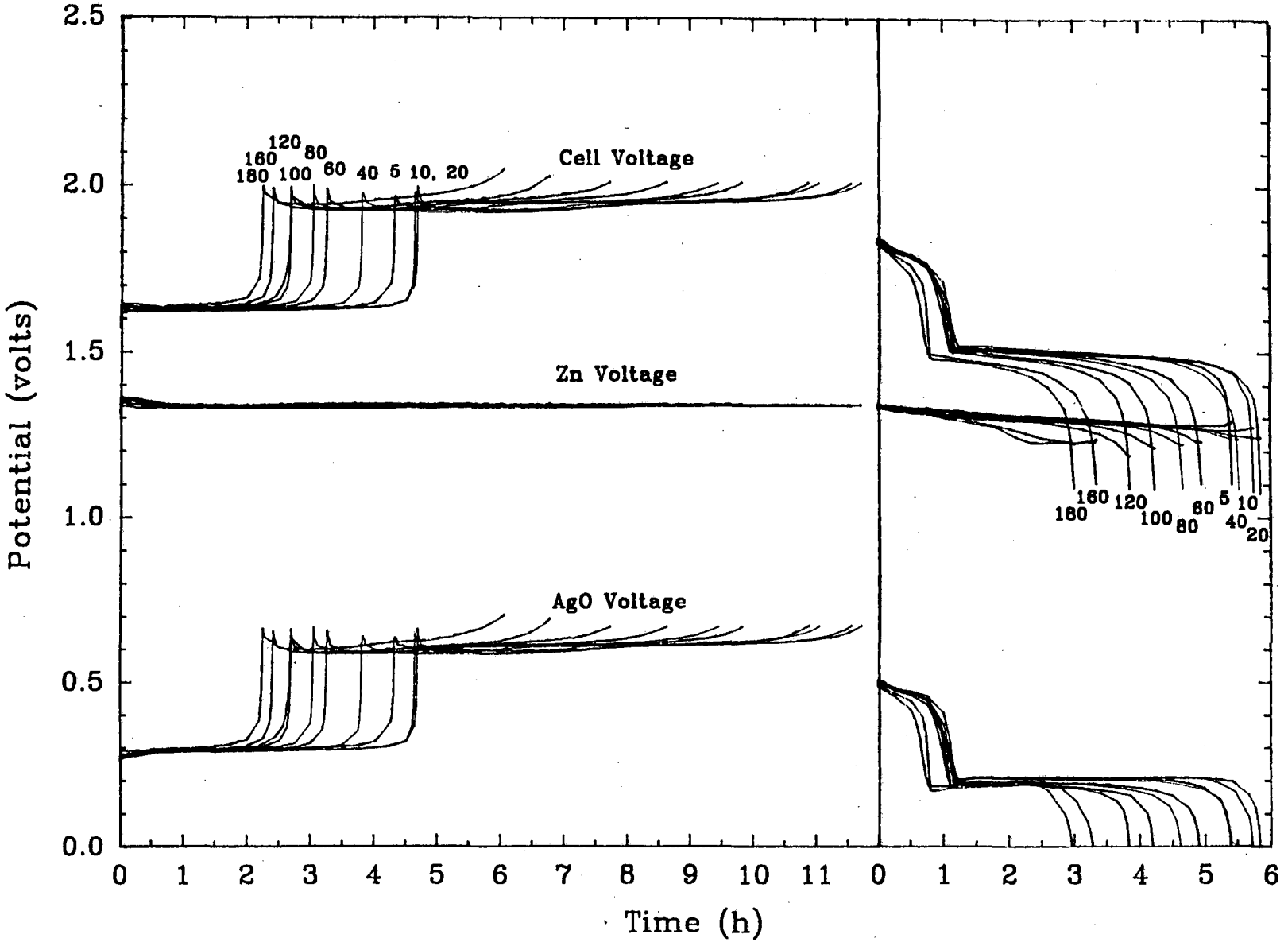

Figure 19 : cell voltage and reference voltages at different cycles for cell C1

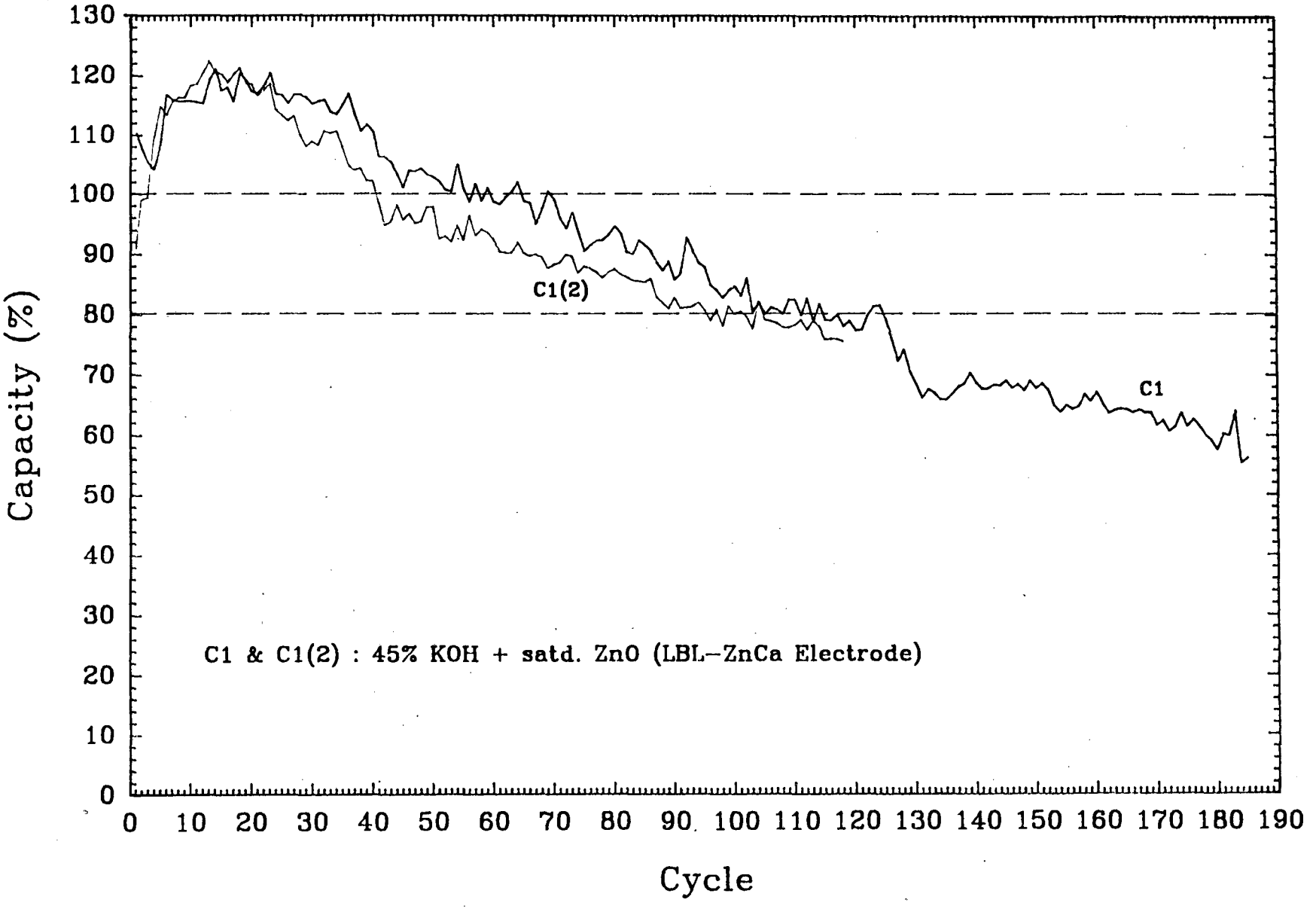

Figure 20 : capacity vs. cycle number for cells C1 and C1(2)

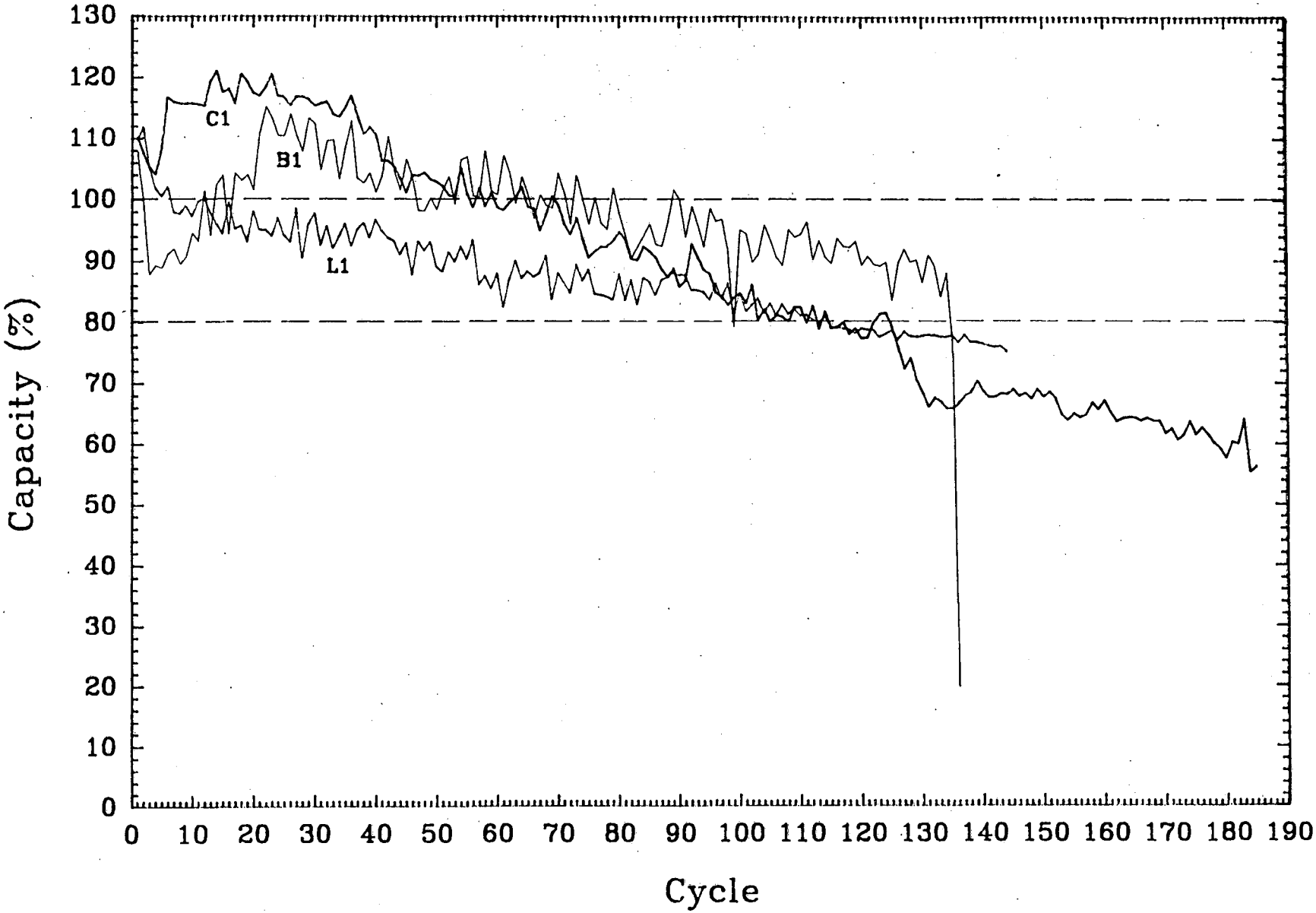

Figure 21 : capacity vs. cycle number for cells B1, L1, and C1

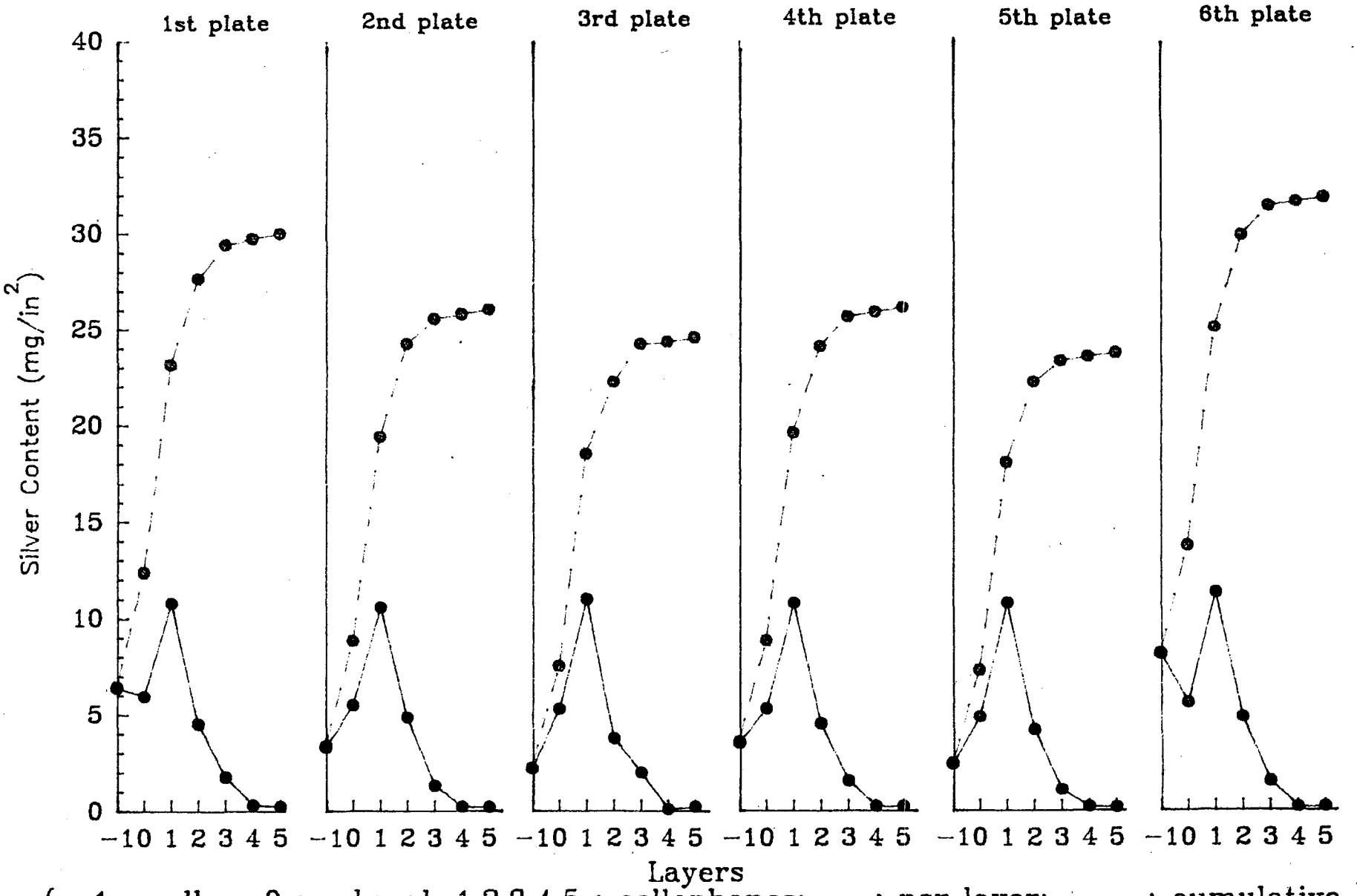

(−1 : pellon, 0 : celgard, 1,2,3,4,5 : cellophanes; —— : per layer; ---- : cumulative)

Figure 22 : silver content in separator system for cell B1 after 136 cycles

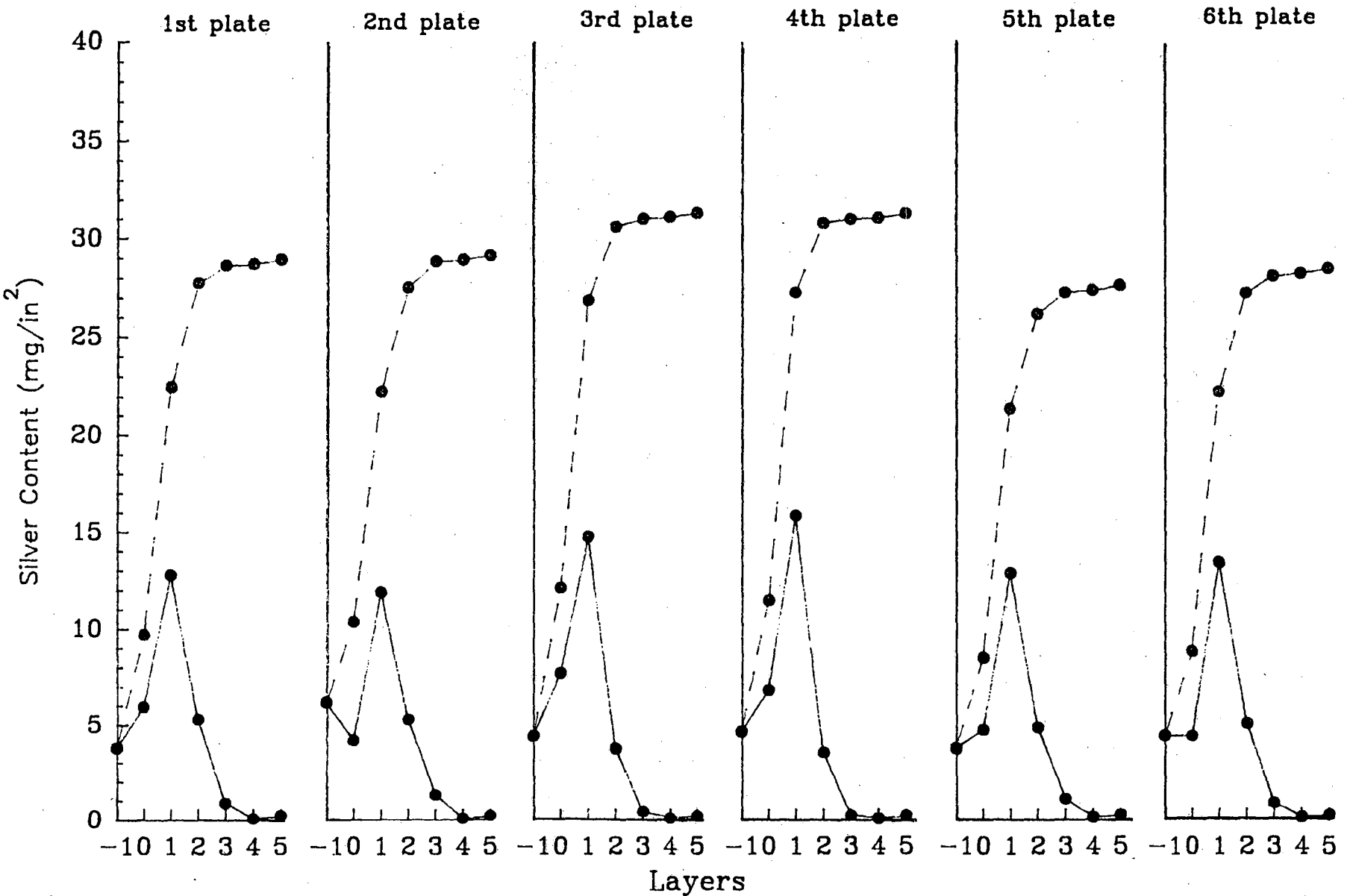

(−1 : pellon, 0 : celgard, 1,2,3,4,5 : cellophanes; —— : per layer; ––– : cumulative)

Figure 23 : silver content in separator system for cell B2 after 97 cycles

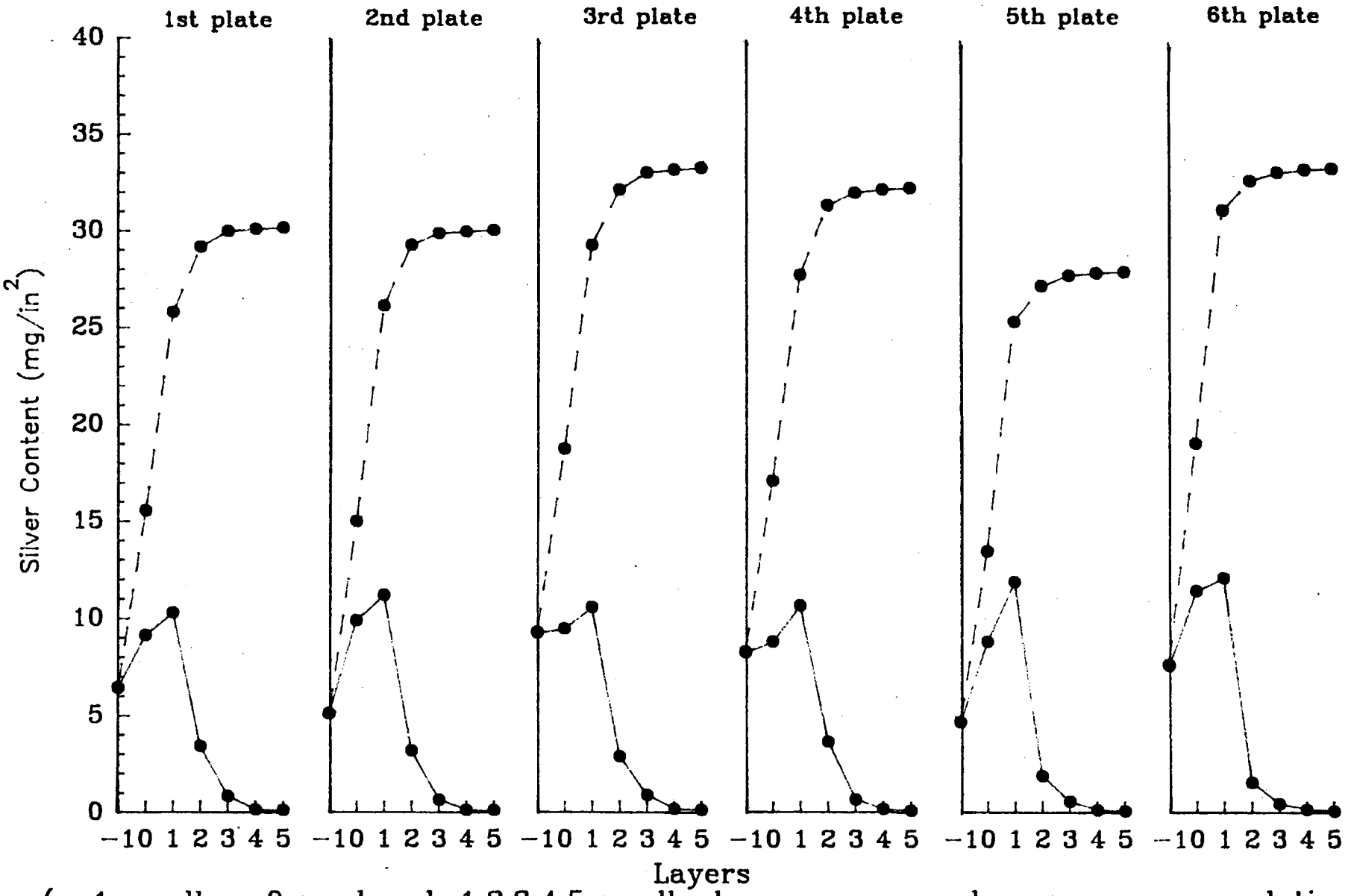

(−1 : pellon, 0 : celgard, 1,2,3,4,5 : cellophanes; —— : per layer; ---- : cumulative)

Figure 24 : silver content in separator system for cell B3 after 58 cycles

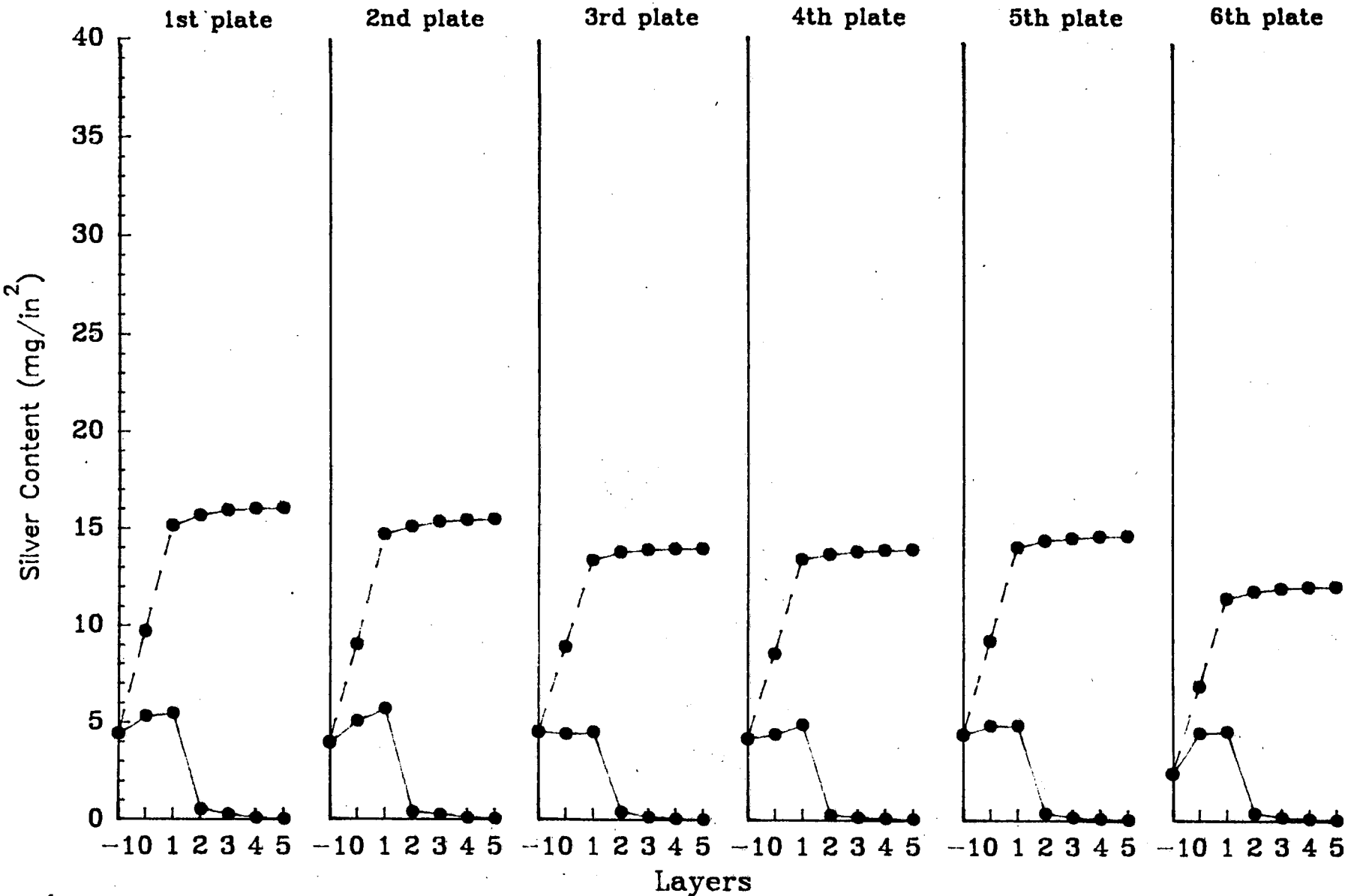

(−1 : pellon, 0 : celgard, 1,2,3,4,5 : cellophanes; —— : per layer; ––– : cumulative)

Figure 25 : silver content in separator system for cell L2 after 45 cycles

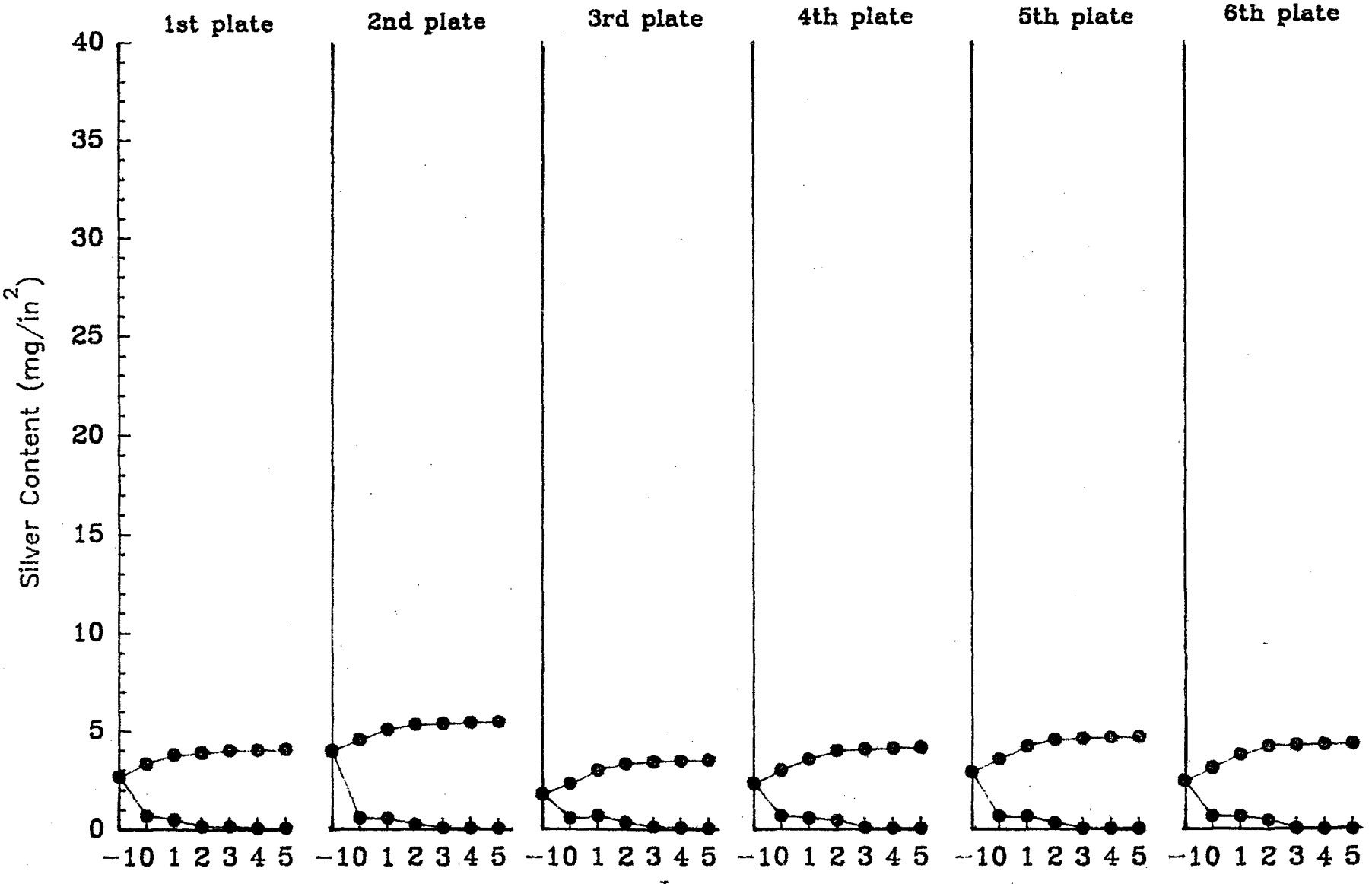

(−1 : pellon, 0 : celgard, 1,2,3,4,5 : cellophanes; —— : per layer; ---- : cumulative)

Figure 26 : silver content in separator system for cell L5 after 21 cycles

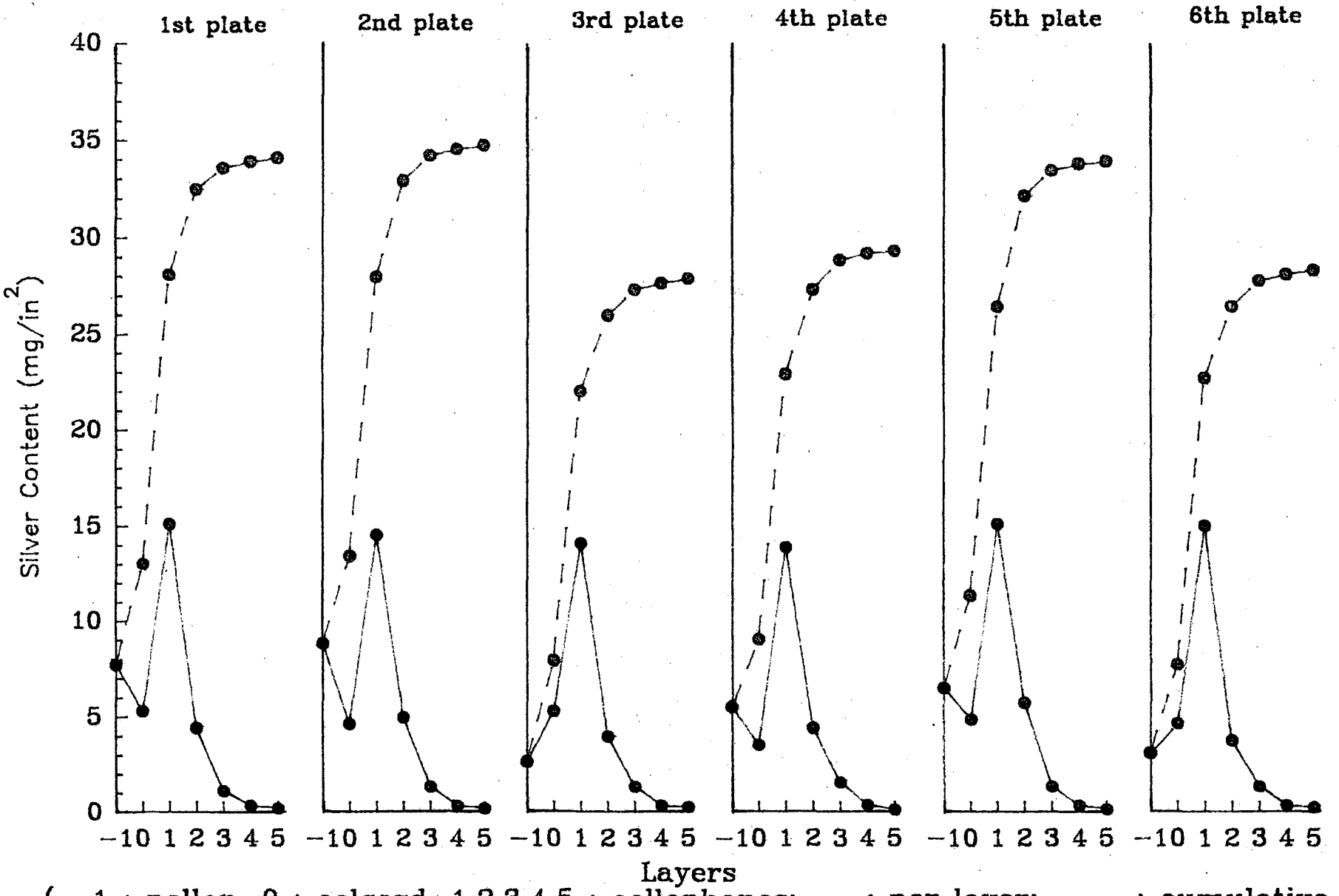

(−1 : pellon, 0 : celgard, 1,2,3,4,5 : cellophanes; —— : per layer; ---- : cumulative)

Figure 27 : silver content in separator system for cell C1 after 185 cycles

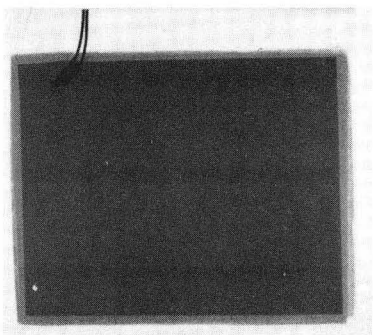

(A)

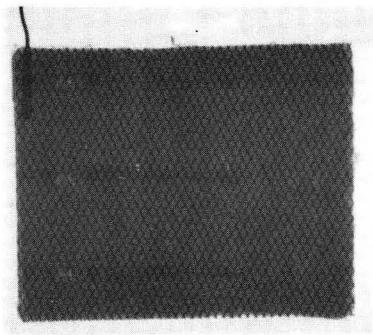

(B)

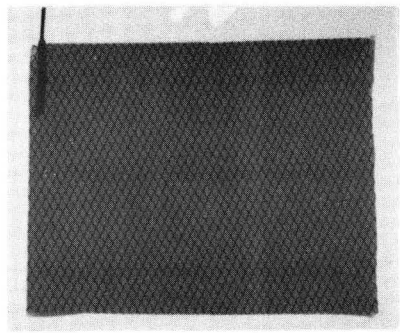

(C)

Figure 28: X-ray photographs of uncycled zinc electrodes.

(a) Zinc electrode fabricated by BST, Inc. (used in the BST cell group); (b) Zinc electrode fabricated by LBL (used in the LBL cell group); and (c) Zinc-calcium electrode fabricated by LBL. (XBB-921-34)

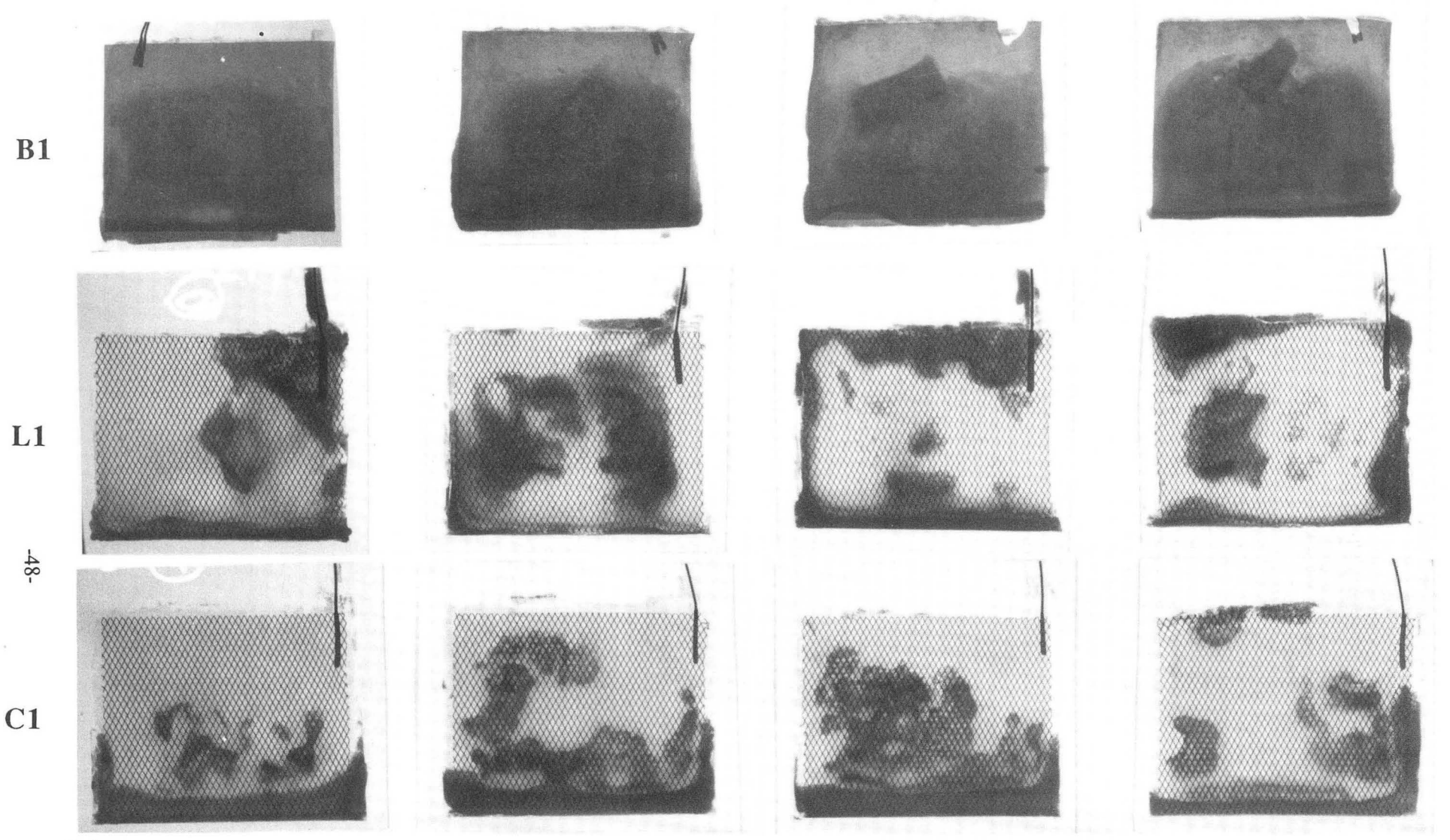

Figure 29: X-ray photographs of representative zinc electrodes harvested from Cells B1 (136 cycles), L1 (145 cycles) and C1 (185 cycles), respectively, shown from top to bottom. From left to right, the images are those of zinc electrode #1 (an electrode nearest to the cell case), zinc electrode #2, zinc electrode #3, and zinc electrode #4 (located at the center of the cell pack). Similar shape-change patterns were seen on the corresponding zinc electrodes harvested from the opposite halves of each cell, *i.e.* zinc electrodes #5, #6 and #7. (XBB-921-35)

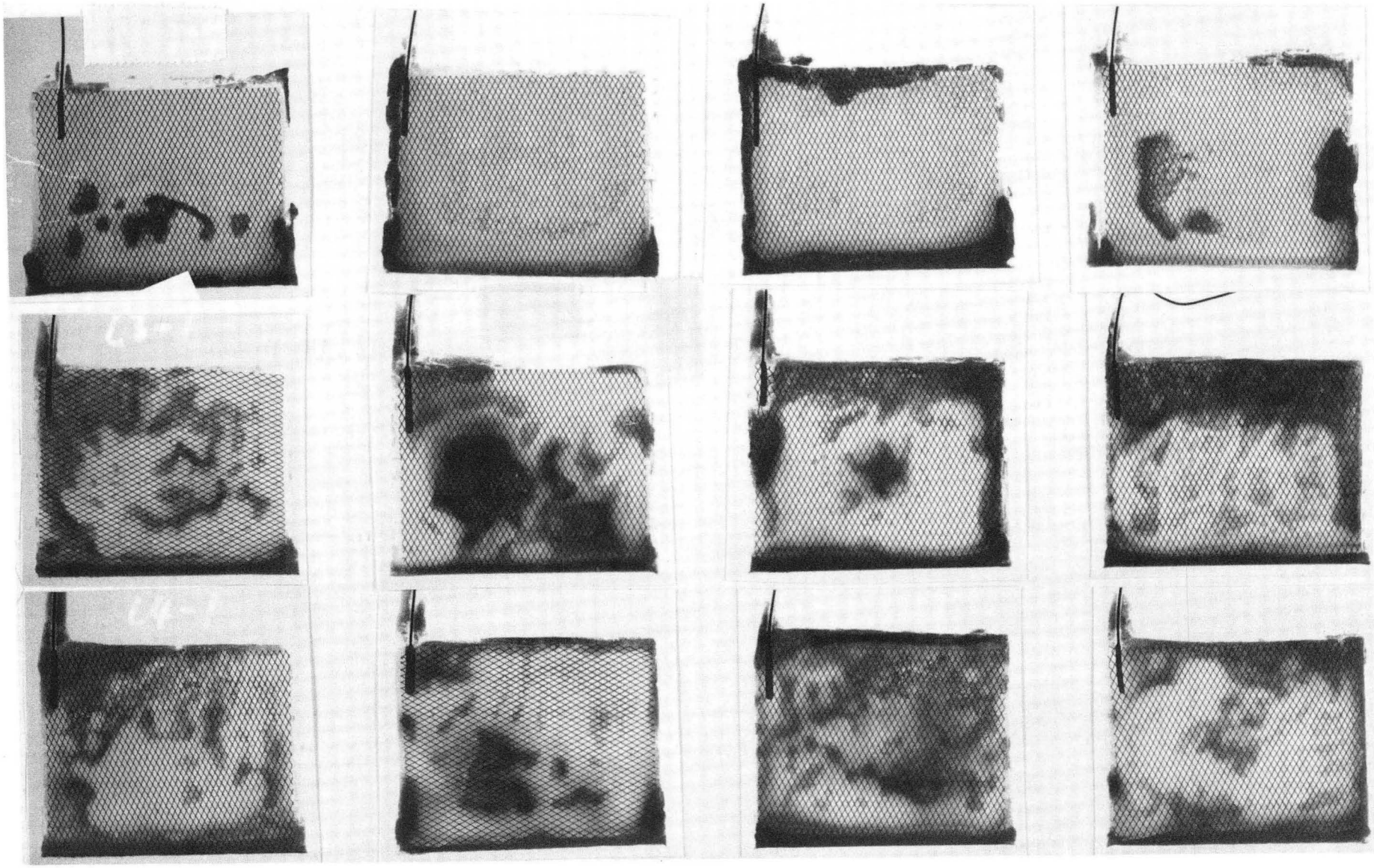

Figure 30: X-ray photographs of representative zinc electrodes harvested from Cells C1(2) (117 cycles), L3 (151 cycles) and L4 (95 cycles), respectively, shown from top to bottom. From left to right, the images are those of zinc electrode #1 (an electrode nearest to the cell case), zinc electrode #2, zinc electrode #3, and zinc electrode #4 (located at the center of the cell pack). Similar shape-change patterns were seen on the corresponding zinc electrodes harvested from the opposite halves of each cell, *i.e.* zinc electrodes #5, #6 and #7. (XBB-921-36)

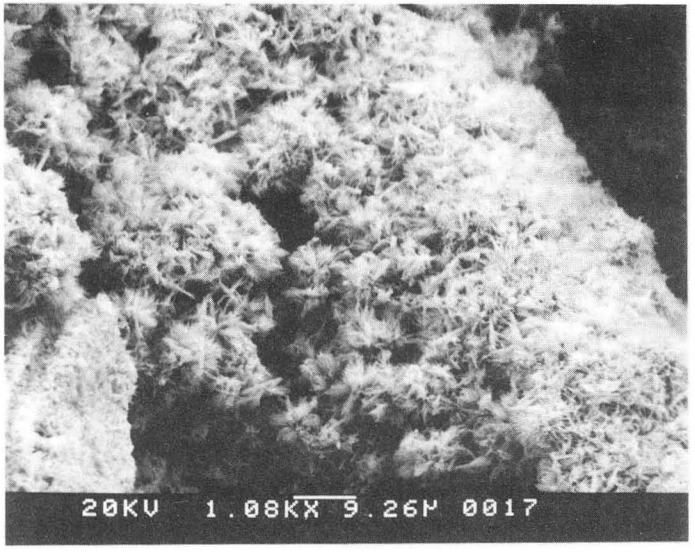

(a) mainly bare current collector with slight residual zinc area

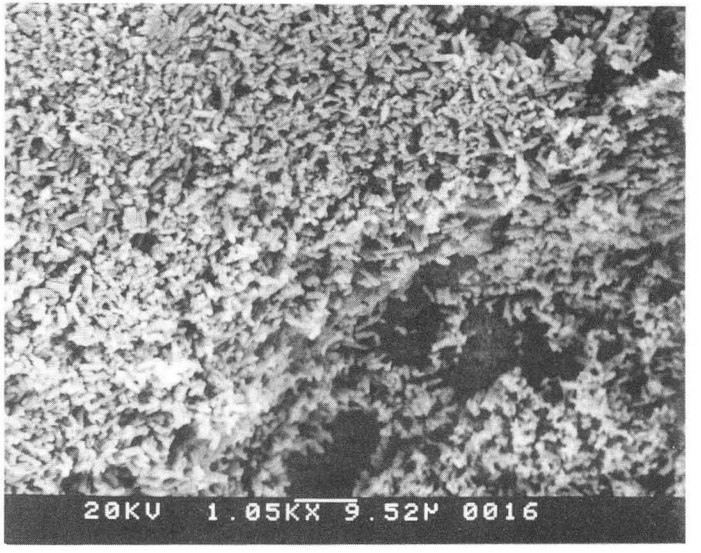

(b) dense area

Figure 31: Morphology of active material in selected areas of a zinc electrode harvested from Cell B1. (XBB 9112-9686)

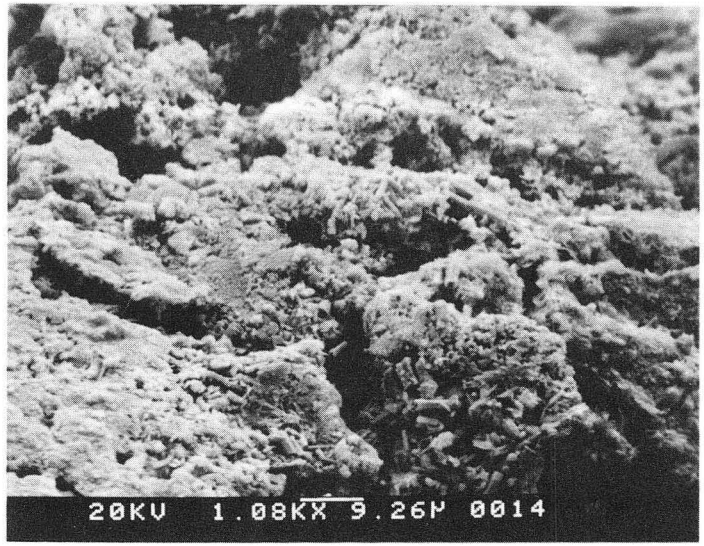

(a) mainly bare current collector with slight residual zinc area

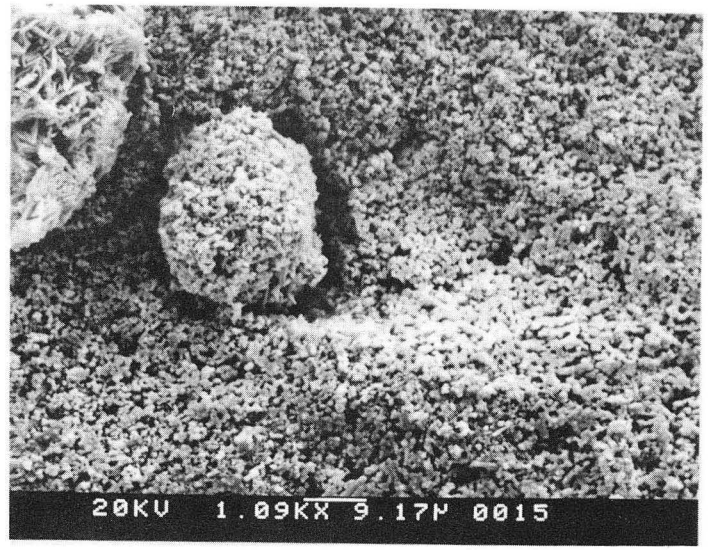

(b) island area

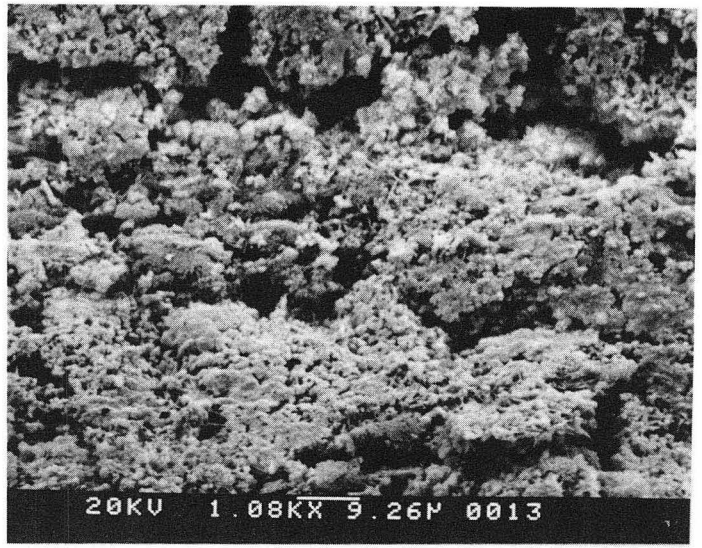

(c) dense area

Figure 32: Morphology of active material in selected areas of a zinc electrode harvested from Cell L1. (XBB 9112-9687)

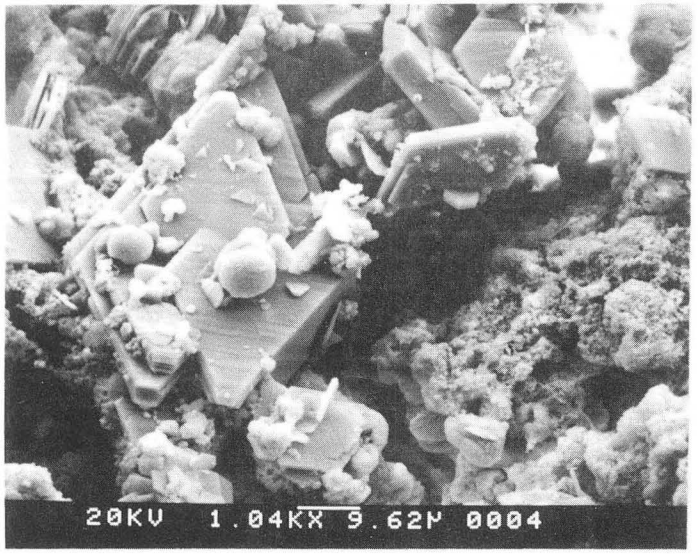

(a) mainly bare current collector with slight residual zinc area

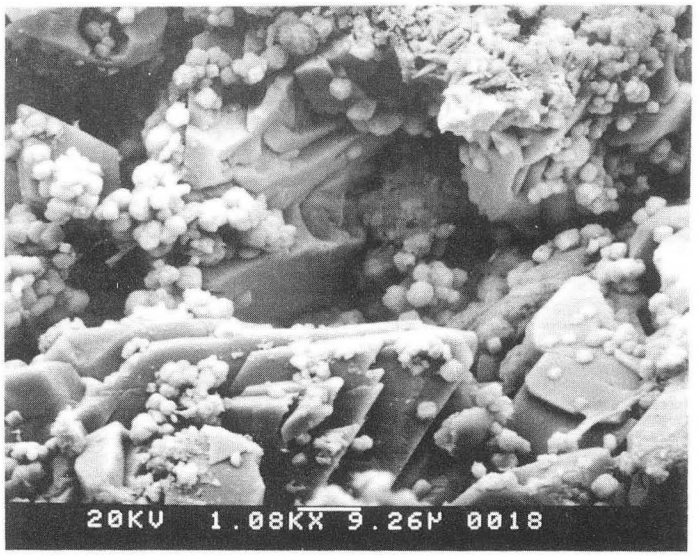

(b) island area

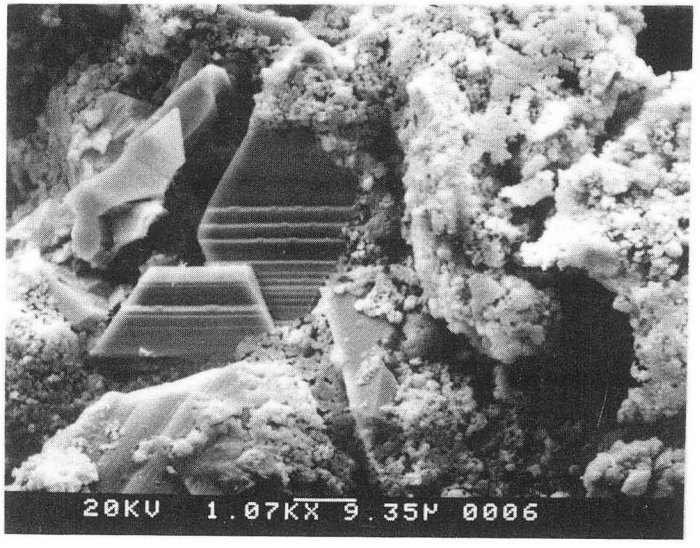

(c) dense area

Figure 33: Morphology of active material in selected areas of a zinc-calcium electrode harvested from Cell C1. (XBB 9112-9685)

LAWRENCE BERKELEY LABORATORY
UNIVERSITY OF CALIFORNIA
TECHNICAL INFORMATION DEPARTMENT
BERKELEY, CALIFORNIA 94720